# Optimizing Fairness in Cellular Networks with Mobile Drone Relays*

Edgar Arribas[a,*], Vincenzo Mancuso[b], Vicent Cholvi[c]

[a] *Universidad San Pablo-CEU, CEU Universities*
[b] *IMDEA Networks Institute*
[c] *Universitat Jaume I*

**Abstract**

Aiding the ground cellular network with aerial base stations carried by drones has experienced an intensive raise of interest in the past years. Reconfigurable air-to-ground channels enable aerial stations to enhance users' access links by means of seeking good line-of-sight connectivity while hovering in the air. In this article, we propose an analytical framework for the 3D placement of a fleet of coordinated drone relays. This framework optimizes network performance in terms of user throughput fairness, expressed through the $\alpha$-fairness metric. The optimization problem is formulated as a mixed-integer non-convex program, which is intractable. Hence, we propose an extremal-optimization-based algorithm, *Parallelized Alpha-fair Drone Deployment* (PADD), which solves the problem online, in low-degree polynomial time. We evaluate our proposal by means of numerical simulations over the real topology of a dense city. We discuss the advantages of integrating drone relay stations in current networks and test several resource scheduling approaches in both static and dynamic scenarios, including with progressively larger and denser crowds.

*Keywords:* Aerial networks, Relay, UAV; Mobile networks, Optimization, $\alpha$-Fairness.

## 1. Introduction

The infrastructure of cellular networks is evolving towards flexible and reconfigurable solutions, able to cope with the highly variable densities of users. Specifically, the current generation of cellular communications, namely 5G [2], embeds new transmission techniques as well as novel communication paradigms, including smart and flexible relaying [3]. Besides, wireless relaying with mobility of relays is possible thanks to precise beamforming and highly efficient cooperative transmission techniques, which makes it possible to operate broadband wireless backhaul links [4]. Without such mature technological tools, many attempts toward mobile relaying have failed in the past, since the advent of broadband wireless data networks [5].

It is therefore currently possible to mount mobile relays on, e.g., transport vehicles and drones, which brings the possibility of moving the network with the users and position relays where the fixed infrastructure cannot sustain the user demand [6, 7]. However, there exist serious concerns on the practicality of mobile relaying, due to interference management problems. For instance, Guo and O'Farrel [8] have derived the capacity of OFDMA cellular networks (like LTE-A, but also in 5G) in the presence of relays reusing cellular frequencies, and showed that relays need to be operated onto orthogonal frequencies. Besides, it is known that using orthogonal frequencies gives additional advantages in terms of simplified resource allocation control [9]. Thus, we study the case of relay drones and base stations (BSs) transmitting on orthogonal frequencies. Specifically, we tackle the optimization of 3D positions for a fleet of coordinated drone relays aiding a set of ground BSs, as depicted in Figure 1, aiming at a fair throughput distribution among users.

We base the optimization on the throughput as evaluated by means of an $\alpha$-fairness metric [10], which is a high-level generalization of fairness metrics, meant to trade-off between pure fairness (i.e., counteracting unequal distribution of

*A preliminary 6-page version of this manuscript appeared in the proceedings of IEEE INFOCOM WKSHPS – MiSARN 2019 [1].

*Corresponding author.
*Email addresses:* edgar.arribas@imdea.org (Edgar Arribas), vincenzo.mancuso@imdea.org (Vincenzo Mancuso), vcholvi@uji.es (Vicent Cholvi)

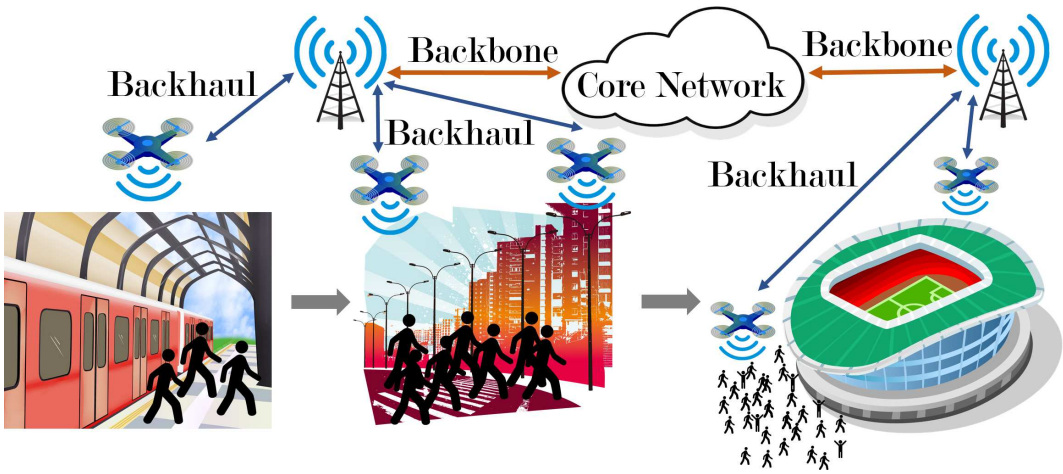


Figure 1: Reference scenario: multi-drone-aided network with people moving from a train station to a football stadium.

individual rewards) and global utilization on a Pareto-efficient curve [11]. The parameter $\alpha$ can be tuned to analytically target, e.g., maximum throughput, proportional fairness or max-min fairness with a single framework and hence find the proper balance between fairness and utilization of resources. In the analysis, we account for the behavior of standard 3GPP networks and user access protocols, and model transmission technology details like the random variations of signal quality received by users over time, the interference caused by relays and BSs, the use of slotted time-frequency resources, the wireless backhaul attachment, and cell selection and resource allocation procedures. Specifically, we adopt stochastic models for path-loss and availability of line-of-sight (LoS) and non-LoS (NLoS) links, and cast our problem into an OFDMA-like resource allocation scheme with several constraints.

The problem of finding the exact optimal drone positions is NP-complete. In particular, our analysis unveils that the role of interference caused by drones and the stochastic characterization of LoS between drones and ground users make the optimization problem intractable. However, is the problem really intractable in practice? To answer this question we analyze the drone-positioning problem under the perspective of a fair maximization of the network throughput provided to mobile users, and unveil its structure, which allows us to find efficient paths towards the computation of near-optimal solutions with low time complexity. Moreover, we show that the most critical part of the problem can be efficiently addressed by leveraging Extremal Optimization (EO) algorithms, which are a class of algorithms specifically designed for polynomial time optimization with intertwined variables [12]. The EO operation is based on picking the "least fit" element of a finite set and change its configuration parameters to improve a global utility function. EO offers a lightweight solution to problems otherwise intractable, and for which researchers proposed genetic algorithms. It is also more reliable than machine learning approaches–e.g., reinforcement learning schemes–since it does not require any training, which would instead be quite heavy and which does not scale with the number of drones to control (the state space in which to train the machine learning algorithm would quickly become unsustainable). We therefore formulate a suitable utility function, targeting $\alpha$-fair user throughput across the network, and design PADD: a Parallelized Alfa-fair Drone Deployment Algorithm. By using an EO algorithm, PADD iteratively updates the position of the least fit drone, i.e., the drone relay that contributes the least to the utility function. We validate our algorithm and evaluate its performance by means of simulations of realistic static and dynamic scenarios. As an illustration of dynamic cases, we evaluate the performance of our algorithm when customers move towards a stadium before a sport event, so that their density grows over time. Beside illustrating the advantages offered by PADD over state of the art algorithms, our numerical results show that optimizing network throughput without considering fairness is not beneficial in dense environments since drones serving the same area generate too much interference.

The contributions of this article are summarized as follows:

- We propose an analytical framework for the 3D placement of a fleet of coordinated drone relays in cellular networks.
- We propose an aerial cellular infrastructure that combines standard 3GPP tools, beamforming techniques, wireless

backhauling and fair resource allocation.

- We show that the analyzed problem is NP-Complete.
- We formulate the 3D placement optimization problem in terms of the $\alpha$-fairness metric to guarantee fair distribution of resources and access link throughputs.
- We propose PADD as an extremal-optimization-based algorithm to solve the problem near-optimally.
- We deterministically solve optimally, in polynomial time, the $\alpha$-fair resource allocation problem for ground-plus-aerial cellular networks.
- We assess and validate our proposal by means of comprehensive numerical results.

The rest of the article is structured as follows. Section 2 discusses related work. Section 3 presents the system model, while Section 4 derives the framework for optimizing drone positions under the $\alpha$-fairness metric. Section 5 describes the design of our optimization algorithm. Section 6 provides numerical results. Section 7 discusses the findings of this article and possible practical implementation issues. Section 8 summarizes and concludes the article.

## 2. Related work

### *2.1. Relay Alternatives*

Mobile and non-terrestrial relays have been investigated in several forms and considering several technologies. For instance, the usage of satellite networks [13] emerged several years ago and is part of 3GPP strategies for evolving cellular networks [14]. However, while satellites serve huge areas, users can only achieve relatively low rates. Moreover, satellites cannot adjust to the user's topology, and service incurs high costs. In contrast, drone relays may move dynamically at low altitudes and serve smaller target regions on demand, where the ground network cannot sustain the high demand from dense spots, so that a swarm of drones is able to rapidly act for aerial connectivity assistance.

Drone relays are also different from fixed relays and Device-to-Device (D2D)-based approaches [15, 16]. In fact, unlike those cases, drone communications are neither fixed nor opportunistic, and the channel propagation is impacted by the probability of communicating with LoS, as we account for in our analysis. That behavior is properly described in [17], where the authors highlight a number of factors that affect the air-to-ground communications.

Thus, in general, satellites, balloons or terrestrial relays cannot face scenarios as the ones studied in this article. In fact, connectivity requirements used to design protocols for satellites, balloons and D2D communications, as well as technology constraints and signal propagation, are radically different from our case. An overview of the recent advances in drone communications, with an emphasis on integrating drones into the fifth-generation of cellular networks can be found in [18].

### *2.2. Drone Position Optimization*

In the recent years there have been various studies that optimize drone relay placement mainly focusing on coverage in static and oversimplified assumptions, as for instance neglecting inter-drone interference [19] or ignoring fairness issues in resource allocation [20]. With that, the resulting problem formulation is simple enough, typically quadratic, yet less realistic than what we derive in this article. In our previous work, we have presented `OnDrone`, a lightweight multi-drone coverage framework that maximizes the number of users covered. In there, we consider Quality-of-Service thresholds and show how to design flying paths for fast repositioning and augmented coverage over time [21]. A similar approach has been followed in [22], where the authors propose the deployment of drones for video surveillance, obtaining a suitable topology (in terms of achieving zero blind spots) with minimum number of drones. However, they assume a region that lacks cellular infrastructure. A different approach is taken in [23], where a Q-learning solution is used to solve the deployment and movement of the drones that maximizes the Quality of Experience [24], although it requires explicit feedback from ground users and protocol changes in the way cells form. Galkin et al. [25] use a stochastic

model to analyze the coverage when drones act as access points for users in urban areas. They demonstrate how the density of the drones determines whether drones should position closer to user hotspots to improve the received signal strength, or further away from one another to mitigate interference. In [26], the authors investigate moving networks of UAVs to extend connectivity and guarantee data rates in the 5G by analyzing possible hovering locations based on limitations such as flight time and coverage. They derived analytic bounds in terms of connectivity and discover two regimes, in function of the existing infrastructure. Furthermore, they identified in which regime the deployment of UAVs is desirable. In [27], the authors propose a communications framework for HetNets composed by macrocells, microcells and communication drones. Although their application scenario is similar to the one of this article, we find remarkable and fundamental differences: they consider only a finite and small set of aerial locations for drones, ignore key communication features such as throughput or coverage and base decisions on minimizing network energy consumption.

The use of drones for the optimization of communication throughput has been explored in recent studies related to various kinds of networks. Here we just mention a few key examples out of an increasingly richer list of publications sprouting in these years.

Hua *et al.* [28] describe how drones can increase the throughput of backscatter networks with their physical presence. Wang *et al.* [29] propose to use drones to support wireless sensor networks optimally by coordinating drone trajectories and by scheduling sensor transmissions. Liang *et al.* [30] model the repositioning of unmanned aerial vehicles (UAV) relays meant to maximize the throughput of mobile communication pairs, with a drone assigned to each pair of devices. Mignardi *et al.* [31] focus on latency and throughput performance of drones using narrowband IoT communications without the presence of terrestrial base stations, whereas Yin and Yu [32] propose resource allocation and trajectory optimization for UAVs that assist cellular networks. However, they do not consider the integration of drone cells and terrestrial base stations, thus solely focusing on drone cell optimization, which is pursued by means of a reinforcement learning algorithm. Indeed, differently from our work, many existing studies do not account for the interaction between drones and ground wireless points of access (e.g., base stations, gateways or relays) and the internal network connectivity bottlenecks (e.g., backhauling and transport limitations).

Some other works do tackle integrated terrestrial and aerial networks. For instance, Liu *et al.* [33] study how to jointly adjust the coverage radius of UAVs and terrestrial base stations by playing with antennas and positions of UAVs, although the main goal of their work consists in maximizing coverage while minimizing coverage overlap and thus reduce the number of required UAVs. Chiaraviglio *et al.* [34] show that solar-energy-supplied UAVs like drones can be also used to assist terrestrial base stations in order to better distribute their resources geographically. They show that the presence of UAVs can significantly increase throughput and reduce energy consumption from the grid. Similar to our work, they assume that UAVs serve users by means of a dedicated frequency, which does not interfere with terrestrial base station transmissions. However, differently from our work, they do not consider relay—as UAVs form independent cells—neither they take into account backhauling constraints, assuming instead that UAVs and terrestrial base station do not compete for resources. Iranmanesh *et al.* [35] consider a drone-logistics network and repurpose drone trajectories to assist the cellular network while performing their primary task (i.e., parcel delivery). They suggest to use D2D to enable drone relay from ground users (uplink) in a congested cell to another ground base station which is not suffering congestion. That work considers the interference between base stations and drones, and assumes that user devices can talk to drones without interfering with base stations because they can use different frequencies. Our work is different, not only because we do not have drone deliveries to take into account, but also because we focus on the downlink rather than uplink, and include backhaul constraints in the problem formulation. The optimization of the relay throughput that a drone can offer is studied in [36], with a single drone providing wireless access in case of disaster, without having to account for interference and other network bottlenecks. The disaster recovery case of multiple drones connected to a single wideband base station in addressed in [37], without optimizing drone positions but rather focusing on the MAC protocol, which is optimized using a matching game.

In [38], the authors tackle the problem of unbalanced traffic distribution in cellular networks by using a UAV-

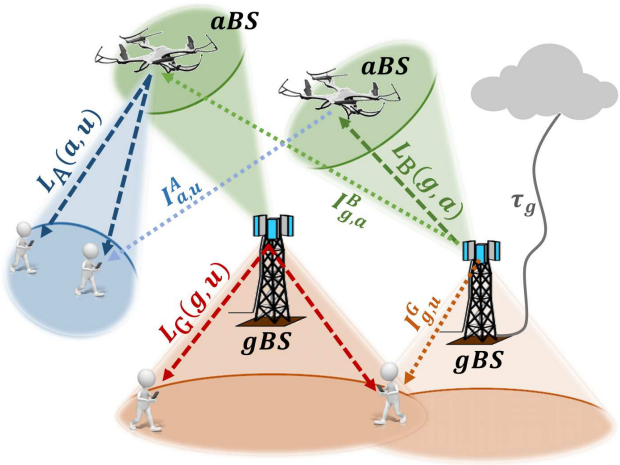


Figure 2: System Model.

assisted wireless network in which the UAV acts as an aerial relay to divert some traffic from the overloaded cell to its adjacent underloaded cell. They jointly optimize UAV position, user association, spectrum allocation, and power allocation to maximize the sum-log-rate of all users in two adjacent cells. First, they design a genetic-based algorithm to optimize the UAV position. Then, they propose an iterative power allocation algorithm based on the sequential convex approximation theory. The authors in [39] investigate the scenario where multiple UAVs cooperatively fly over heterogeneous ground users and collect data without a central controller. They jointly optimize the trajectories of UAVs and the ground users associations to maximize total throughput and energy efficiency, taking into account both signal-to-interference-and-noise ratio and fairness among users. By means of simulations, they demonstrate that the proposed algorithm outperforms commonly adopted schemes, in terms of fair throughput and energy consumption.

Although all these works provide valuable contribution and foundational results, they do not shed light on problems like capacity optimization with fairness targets when a fleet of drones is deployed to assist a cellular network with realistically coupled access and backhaul resources, which is our goal in this article. Neither they provide a realistic framework to integrate drone relay stations into current cellular networks, whereas we show that our practical approach accounts for integration. In the conference version of this article [1], we address this problem from a quite simple approach: in there, we relax critical constraints like wireless backhaul and backbone bottlenecks, and air-space constraints where drones can be located. Such simplifications allow for the design of a simpler system model and less complex algorithms and optimizations, yet bring the risk of being inaccurate. In this article, instead, we provide a fully general, realistic, precise and tractable model for an aerial network integrated in a cellular infrastructure.

Besides, here we use EO in a novel way. EO algorithms took relevance on fields as biology or physics, and have been also applied to network science, e.g., to optimize transport in complex networks [40]. EO has been thought and used so far as a form of centralized static optimization. Instead, in this article we use EO to design an algorithm that works in parallel threads and dynamically, as the system evolves.

## 3. System Model

Our goal is to derive an analytical framework that finds optimal 3D locations of drone relays, given the position of users and ground stations, so as to optimize downlink communications. We target $\alpha$-fair instantaneous user throughput. To this aim, jointly with path-loss and interference in both access and backhaul, we address how users perform cell selection and get resources allocated. The modelled system is a plain 3GPP cellular system comprising access and backhaul networks, with drones acting as standard 5G relays [41].

In order to illustrate the system model and parameters involved in the network, we show the main components in Figure 2 and describe the meaning of the parameters in Table 1.

Table 1: System model parameters

| Parameter | Description |
|---|---|
| $\alpha$ | Fairness level |
| $A_g$ | Maximum number of *aBS*s that *gBS* $g$ can serve |
| $\mathcal{A}$ | Set of *aBS*s |
| $\mathcal{B}$ | Set of BSs, i.e., set of *aBS*s and *gBS*s jointly |
| $\mathcal{G}$ | Set of *gBS*s |
| $\gamma^{\mathcal{A}}_{a,u}$ | SINR of aerial access link $(a,u)$ |
| $\gamma^{\mathcal{B}}_{g,a}$ | SINR of aerial backhaul link $(g,a)$ |
| $\gamma^{\mathcal{G}}_{g,u}$ | SINR of ground access link $(g,u)$ |
| $I^{\mathcal{A}}_{a,u}$ | Interference from *aBS* $a$ to UE $u$ |
| $I^{\mathcal{B}}_{g,a}$ | Interference from *gBS* $g$ to *aBS* $a$ |
| $I^{\mathcal{G}}_{g,u}$ | Interference from *gBS* $g$ to UE $u$ |
| $L_{\mathcal{A}}(a,u)$ | Loss of air-to-ground channel from *aBS* $a$ to UE $u$ |
| $L_{\mathcal{B}}(g,a)$ | Loss of ground-to-air channel from *gBS* $g$ to *aBS* $a$ |
| $L_{\mathcal{G}}(g,u)$ | Loss of ground-to-ground channel from *gBS* $g$ to UE $u$ |
| $\phi_{g,a}$ | Angle from main lobe of *gBS* $g$ to *aBS* $a$ |
| $P_{LoS}(a,u)$ | LoS-likelihood of link $(a,u)$ |
| $U_{\max}$ | Maximum number of UEs a BS can serve |
| $W_{\mathcal{A}}$ | Available bandwidth of aerial access channels |
| $W^{\min}_{\mathcal{A}}$ | Minimum bandwidth guaranteed to aerial access links |
| $W_{\mathcal{B}}$ | Available bandwidth of aerial backhaul channels |
| $W^{\min}_{\mathcal{B}}$ | Minimum bandwidth guaranteed to aerial backhaul links |
| $W_{\mathcal{G}}$ | Available bandwidth of ground access channels |
| $W^{\min}_{\mathcal{G}}$ | Minimum bandwidth guaranteed to ground access links |
| $\tau_g$ | Backbone capacity of *gBS* $g$ |

### *3.1. Reference Scenario*

We consider a flat ground surface $\mathcal{S}$ where a set $\mathcal{G}$ of $G$ ground base stations (*gBS*) provide cellular service. The position of each *gBS* $g$ is denoted as $\Pi^g = (X^g, Y^g)$. We assume that every *gBS* $g$ is wired to the internet with a backbone capacity $\tau_g$. We consider that a set $\mathcal{U}$ of $U$ user equipments (UEs) is on the ground, requesting cellular service. We denote the position of each user $u$ as $\pi_u = (x_u, y_u)$. The network disposes of a fleet $\mathcal{A}$ of $A$ aerial base stations (*aBS*) that act as mobile relays. Each *aBS* is mounted on a drone (for ease of readability, we may refer just as "drone" to an *aBS*). We assume that the system operator disposes of two frequency bands to offer user access: the first band is used by *gBS*s to provide both cellular access to ground users and backhaul connectivity to *aBS*s; and the second band is used by *aBS*s to provide cellular access to ground users. This assumption mimics the common scenario in which an operator deploys different types of base stations and equip them with different frequencies to simplify network management. Indeed, it is common that an operator disposes of multiple licenses to use more than one cellular band. It is also common practice to coordinate transmissions from different base stations, especially in case of mixed deployments with macro and small cells. Frequency reuse is one of the possible and simplest schemes to use for coordination, which is what we adopt for simplicity. Nonetheless, please note that the analysis carried out in this article can be extended to the case of using a single frequency for all transmissions or any arbitrary number of frequencies (e.g., one per aerial and ground base station, in the most extreme case).

Under our assumptions, users connected to drones suffer no interference from *gBS*s. Similarly, users connected to ground base stations are not interfered by drone transmissions. Drones fly in the air space, so that we denote as

$\Pi_a = (X_a, Y_a, h_a)$ the 3D position of drone $a$. We denote as $\mathcal{B} = \mathcal{G} \cup \mathcal{A}$ the set of all the base stations (*gBS*s jointly with *aBS*s) that form the whole network.

We assume that *gBS*s reuse the downlink spectrum used for the *gBS*–UE access links in order to provide backhaul wireless service to *aBS*s. Usually, *gBS*s dispose of three antenna sectors pointing mainly to the ground in order to provide cellular coverage to users. In addition to these antennas, we assume that *gBS*s dispose of an additional full dimensional antenna array that performs 3D-beamforming over clear LoS links in order to establish *gBS*–*aBS* links for backhauling, as suggested and studied in [42]. Hence, *gBS*–UE and *gBS*–*aBS* links do not practically interfere. Moreover, 3D antenna arrays allow *gBS*s to relay traffic to several drones, by alternating transmissions every few milliseconds. Therefore, we assume that each *gBS* can set backhaul wireless links with more than one *aBS*, and we also assume that a minimum backhaul bandwidth $W_{\mathcal{B}}^{\min}$ is guaranteed, which implies that only a limited number of drones can stay connected to a single ground base station.

In order to analyze a realistic network configuration, differently from what we assume for BSs talking to each other, we do not assume that transmissions to users can benefit from beamforming, therefore, we account for inter-cell interference for the groups of users connected to the same type of BS, be it *aBS* or *gBS*. We do so because beamforming to users requires non-negligible overheads to track the position of erratically moving users, and to fine tune the beam within potentially narrow spaces crowded with users. Instead, *aBS*s and *gBS* can easily have precise information about their positions at any time, and do not risk to stay packed in small spaces. Having said that, our analysis can be straightforwardly simplified to apply also to the ideal case in which all transmissions can be interference-free due to beamforming, should that possibility become reality, as foreseen for future 3GPP networks and other cellular systems.

Another important aspect to consider in drone-assisted missions is the energy consumption management of drones. Ths is generally enforced by means of a recharge strategy and with additional backup drones. In this article, we assume that $A$ drones are guaranteed to be operational in a desired position when the optimization is run. Hence, we assume that there is a parallel recharge scheduling strategy that uses a minimum number of extra drones to guarantee a persistent communications service with $A$ *aBS*s at any moment. This parallel mechanism can certainly be achieved, as we have already proposed and demonstrated in [43].

### *3.2. Channel Modelling*

We assume that the network operator disposes of two orthogonal frequency bands. One band is assigned to *gBS*s to provide access service to ground users as well as aerial backhaul service to *aBS*s, with a fixed bandwidth $W_{\mathcal{G}}$ and $W_{\mathcal{B}}$, respectively. The other band is assigned to *aBS*s for aerial user access and it has a fixed bandwidth $W_{\mathcal{A}}$. Hence, we model three different kinds of channels: (i) air-to-ground and (ii) ground-to-ground channels in the access network, and (iii) ground-to-air channels in the backhaul network.

To optimize the network and compute link throughputs we need to compute the signal strength of each wireless channel, measured as the SINR. In order to compute the SINR, we study path-loss and fading of channels, as well as suffered interference. Then, throughputs will be estimated with the well-known Shannon formula.

The notation of each parameter of the channel model can be found in Table 1, and the mathematical details of the modelling of each kind of channel can be found in separate sections of Appendix A.

**Air-to-ground access channels.** The loss of these channels differs notably depending on whether links are free of obstacles [44]. Hence, this loss depends on the LoS-likelihood [45] of links. As *aBS*s serve users in OFDMA channels, these users do not interfere among themselves. However, users suffer aggregated interference from other *aBS*s serving other users. We denote the loss from *aBS* $a$ to UE $u$ as $L_{\mathcal{A}}(a, u)$.

**Ground-to-ground access channels.** The loss of these channels follows the well-known path-loss model with slow fading [46]. As *gBS*s serve users in OFDMA channels, there is no intra-cell interference. However, we account for inter-cell interference from neighbor ground cells. We denote the loss from *gBS* $g$ to UE $u$ as $L_{\mathcal{G}}(g, u)$.

**Ground-to-air backhaul channels.** Since backhaul links follow directional beams in LoS, the loss of these channels also follows the well-known path-loss model with slow fading [46]. Backhaul links reuse the spectrum from the

Table 2: Optimization variables & parameters.

| Variable | Description |
|---|---|
| $B^{g,a}$ | Binary variable for the existence of backhaul link $(g, a)$ |
| $C_{a,u}$ | Binary variable for the existence of access link $(a, u)$ |
| $C_u^{g_u}$ | Binary variable for the existence of access link $(g_u, u)$ |
| $\Pi_a$ | Aerial position of *aBS* $a$ |
| $\mathcal{S}_a$ | Air space restricted to *aBS* $a$ |
| $T_{b,u}$ | Throughput allocated to access link $(b, u)$ |
| $T^{g,a}$ | Throughput allocated to backhaul link $(g, a)$ |
| $W_{b,u}$ | Bandwidth allocated to access link $(b, u)$ |
| $W^{g,a}$ | Bandwidth allocated to backhaul link $(g, a)$ |

ground access channels. However, *gBS*s perform 3D beamforming for backhauling and hence there is no interference between ground access and aerial backhaul. Still, other *gBS*s might serve other *aBS*s in a beamforming direction such that served *aBS*s suffer interference (attenuated depending on the radiating angle). We account for such interference. We denote the loss from *gBS* $g$ to *aBS* $a$ as $L_{\mathcal{B}}(g, a)$.

### *3.3. Cell Selection and Resource Allocation*

BSs cannot provide service to unlimited numbers of users because $(i)$ available radio resources are limited and $(ii)$ it is necessary to guarantee a minimum set of radio resources to each connected user, to guarantee signaling exchange with the BS; this is needed to schedule data transmissions to and from the BS. Of course, the number of devices is also limited by the minimum bandwidth that the system aims to guarantee to each user. Therefore, in general, the maximum number of users that can be simultaneously served is limited, and we denote by $U_{\max}$ such number.

**Cell Selection.** We assume that users perform cell selection as in currently operational 3GPP networks: first, UEs select the BS with strongest Signal-to-Noise Ratio (SNR); if the request is rejected because channel conditions deteriorate or the BS runs at maximum capacity, then the UE performs cell re-selection, and tries to attach to the BS with next strongest SNR, and so on until the user gets attached [47].

**Resource Allocation.** We assume that *gBS*s and *aBS*s schedule cellular users according to an OFDMA system. Today's BSs use an OFDMA system and dispose of a finite set of physical resource blocks organized in subframes, which repeat to form frames lasting a few milliseconds (1 to 10 ms in 3GPP-compliant networks). A physical resource block is the smallest unit of time-frequency resources that can be allocated to a user. Thus, we assume that the minimum bandwidth allocated to a user is the bandwidth corresponding to one resource block and the scheduler guarantees that each user receives, on average, at least one block per subframe in each OFDMA frame. We denote as $W_{\mathcal{G}}^{\min}$ and $W_{\mathcal{A}}^{\min}$ the minimum bandwidth that a *gBS* or an *aBS* can allocate to a single user.

Backhaul links also use an OFDMA system, although *aBS*s select a *gBS* according to a global network optimization criterion, rather than based on SNR. Moreover, *gBS*s can serve $A_g$ *aBS*s at most, and each backhaul link $(g, a)$ disposes of a minimum bandwidth $W_{\mathcal{B}}^{\min}$, to relay traffic.

## 4. Optimization

Here we derive an analytic framework for the 3D positions of *aBS*s, to optimize throughputs based on $\alpha$-fairness [10]. We seek optimal *aBS* positions and BS–UE associations, and also optimal backhaul association and optimal allocation of physical resources. We formally present the optimization problem addressed in this article:

***Throughput Problem $\mathcal{T}$****: Given a set $\mathcal{G}$ of $G$ fixed gBSs, a fleet $\mathcal{A}$ of $A$ relay aBSs hovering at heights in the range $[h_{\min}, h_{\max}]$, a set $\mathcal{U}$ of $U$ ground UEs that may connect to either a gBS or an aBSs, each of which can serve $U_{\max}$ UEs*

$$\max_{\substack{\Pi_a, C_{a,u}, W_{b,u},\\ B^{g,a}, W^{g,a}}} \quad U^{\alpha}_{thr} = \begin{cases} \sum\limits_{u\in\mathcal{U}} \left( \sum\limits_{b\in\mathcal{B}} T_{b,u} \right)^{1-\alpha} \cdot \frac{1}{1-\alpha}, & \alpha \neq 1; \\ \sum\limits_{u\in\mathcal{U}} \log\left( \sum\limits_{b\in\mathcal{B}} T_{b,u} \right), & \alpha = 1; \end{cases}$$

s.t.:

*gBS–aBS association constraints:*

$$\sum_{g\in\mathcal{G}} B^{g,a} = 1, \quad \sum_{a\in\mathcal{A}} B^{g,a} \leq A_g, \qquad \forall g \in \mathcal{G}, \forall a \in \mathcal{A};$$

*gBS–aBS capacity constraints:*

$$W^{\min}_{\mathcal{B}} \cdot B^{g,a} \leq W^{g,a} \leq W_{\mathcal{B}} \cdot B^{g,a}, \qquad \forall g \in \mathcal{G}, \forall a \in \mathcal{A};$$
$$\sum_{a\in\mathcal{A}} W^{g,a} \leq W_{\mathcal{B}}, \qquad \forall g \in \mathcal{G};$$
$$T^{g,a} \leq W^{g,a} \log_2\left(1 + \gamma^{\mathcal{B}}_{g,a}\right), \qquad \forall g \in \mathcal{G}, \forall a \in \mathcal{A};$$

*gBS backbone constraint:*

$$\sum_{a\in\mathcal{A}} T^{g,a} + \sum_{\substack{u\in\mathcal{U}:\\ g=g_u}} T_{g,u} \leq \tau_g, \qquad \forall g \in \mathcal{G};$$

*BS–UE association constraints:*

$$C^{g_u}_u + \sum_{a\in\mathcal{A}} C_{a,u} = 1, \qquad \forall u \in \mathcal{U};$$
$$\sum_{\substack{u\in\mathcal{U}:\\ g=g_u}} C^g_u \leq U_{\max}, \quad \sum_{u\in\mathcal{U}} C_{a,u} \leq U_{\max}, \qquad \forall g \in \mathcal{G}, \forall a \in \mathcal{A};$$

*gBS–UE capacity costraints:*

$$W^{\min}_{\mathcal{G}} \cdot C^{g_u}_u \leq W_{g_u,u} \leq W_{\mathcal{G}} \cdot C^{g_u}_u, \qquad \forall u \in \mathcal{U};$$
$$\sum_{u\in\mathcal{U}} W_{g,u} \leq W_{\mathcal{G}}, \qquad \forall g \in \mathcal{G};$$
$$T_{g_u,u} \leq W_{g_u,u} \log_2\left(1 + \gamma^{\mathcal{G}}_{g_u,u}\right), \qquad \forall u \in \mathcal{U};$$

*aBS–UE capacity constraints:*

$$W^{\min}_{\mathcal{A}} \cdot C_{a,u} \leq W_{a,u} \leq W_{\mathcal{A}} \cdot C_{a,u}, \qquad \forall a \in \mathcal{A}, \forall u \in \mathcal{U};$$
$$\sum_{u\in\mathcal{U}} W_{a,u} \leq W_{\mathcal{A}}, \qquad \forall a \in \mathcal{A};$$
$$T_{a,u} \leq W_{a,u} \log_2\left(1 + \gamma^{\mathcal{A}}_{a,u}\right), \qquad \forall a \in \mathcal{A}, \forall u \in \mathcal{U};$$
$$\sum_{u\in\mathcal{U}} T_{a,u} \leq \sum_{g\in\mathcal{G}} T^{g,a}, \qquad \forall a \in \mathcal{A};$$

*Air space constraint:* $\Pi_a \in \mathcal{S}_a, \qquad \forall a \in \mathcal{A}.$

Figure 3: Fair Throughput Optimization Program.

*at most, find the optimal position of each aBS $a \in \mathcal{A}$, the optimal user association, the optimal backhaul association and the optimal user resource allocation so to maximize the $\alpha$-fair throughput utility function.*

We formulate the drone positioning problem as a Mixed-Integer Non-Convex Program (MINCP) in Figure 3. The meaning of all the optimization variables is shown in Table 2.

On the access network side, we denote as $C_{a,u} \in \{0,1\}$ the decision variable that tells whether $u$ connects to *aBS* $a$. Similarly, $C^{g_u}_u \in \{0,1\}$ tells whether $u$ connects to *gBS* $g_u$. Decision variables $W_{b,u}$ and $T_{b,u}$ denote bandwidth and throughput allocated to link $(b,u)$. Throughput is a decision variable and not directly computed with the Shannon formula, since, in addition to bandwidth limitations we must account for access, backhaul and backbone bottlenecks.

On the backhaul network side, we denote as $B^{g,a} \in \{0,1\}$ the decision variable that tells whether *aBS* $a$ is attached to *gBS* $g$. Variables $W^{g,a}$ and $T^{g,a}$ denote bandwidth and throughput of the backhaul link $(g,a)$, respectively.

*Network utility and constraints*

The utility function of the optimization problem in Figure 3 corresponds to the $\alpha$-fairness metric. This utility function is additive in terms of utilities conveyed by single BSs. Depending on the value of $\alpha \geq 0$, known as the $\alpha$-fairness level, the metric captures different fairness criteria such as proportional fairness ($\alpha = 1$), max-min fairness ($\alpha \to +\infty$) or the maximum capacity ($\alpha = 0$). Specifically, as derived in [10], a system with rates $T$ is proportionally fair if for any other system of rates $T'$, the aggregate proportional change in the rates is negative, while a system with rates $T$ is said to be max-min fair if any rate $T_i$ cannot be increased without decreasing some smaller $T_j$. However, it might be controversial what is a fair rate allocation for a given network, since the network needs to find a balance between fairness and utilization of resources. In order find a desired trade-off between utilization of resources and maximum fairness, the tunable parameter $\alpha$ generalizes all fairness metrics in the following sense: if $\alpha = 1$, the $\alpha$-fairness metric is proportionally fair, hence prioritizing the utilization of resources, but as long as $\alpha$ becomes larger, more priority is given to fairness. In general, for any choice of $\alpha \geq 0$, the larger $\alpha$ the higher the importance of fairness over utilization in the resulting utility metric [11], and an $\alpha$-fair system of rates $T$ is that system in which for any other system of rates $T'$, the aggregate of the changes of rates relative to the $\alpha$-power of $T$ is negative. Optimizing for different values of $\alpha$ corresponds to assign different levels of importance to individual fairness over global utilization goals. In particular, $\alpha = 0$ leads to optimize the global utility only, while as $\alpha$ increases the relative importance of fair distribution of utilities grows monotonically until, as $\alpha \to \infty$, the utilization plays no role in the optimization.

Constraints in Figure 3 correspond to the following restrictions:

***gBS–aBS* association constraints** state that every *aBS* must associate with one *gBS* to set a wireless backhaul link, and that every *gBS* can serve at most $A_g$ *aBS*s.

***gBS–aBS* capacity constraints** impose guarantees on bandwidth and throughput allocation on backhaul links.

The ***gBS* backbone constraint** restricts every *gBS* to provide connected *aBS*s and connected users with an aggregated throughput not higher than the capacity $\tau_g$ of the backbone link that serves that *gBS*.

**BS–UE association constraints** state that each user can associate only to one BS, either a ground station or a drone, and that the maximum allowed number of UEs served by each BS is limited to $U_{\max}$.

***gBS*–UE capacity constraints** impose guarantees on bandwidth and throughput allocation on *gBS*–UE links.

***aBS*–UE capacity constraints** impose guarantees on bandwidth and throughput allocation on *aBS*–UE links, while at the same time the throughput of a user cannot exceed the backhaul link capacity and the aggregate user throughput cannot exceed the backhaul throughput.

The **Air space constraint** delimits the 3D air space within which an *aBS* can be moved, $\mathcal{S}_a$, and which is a ball centered in the current position of the drone with a radius equal to the distance that the drone can fly within a fixed time (i.e., time itself is the real constraint).

Modeling air-to-ground connections brings unavoidable non-convex functions, so that the formulated problem is not tractable with currently available optimizers, which are able to deal *only* with problems that are convex.

*Feasibility and NP-Completeness*

Here we remark that the formulated optimization problem in Figure 3 *always* admits a feasible solution. We just have to place each *aBS* $a \in \mathcal{A}$ randomly in each $\mathcal{S}_a$, attach each UE and *aBS* to a random *gBS*, allocate to each UE and *aBS* the minimum allocable bandwidth and assign null throughputs to every link in the network. This naive network setting is always a feasible solution of the problem.

Moreover, the problem of finding the exact optimal drone positions is NP-Complete. Indeed, the NP-Complete Minimum-Geometric Disk-Cover (MGDC) problem [48] can be reduced, in polynomial time, to a special instance of the problem in which users get 1 bps if a drone serves them and 0 bps otherwise. This result is a direct consequence of the NP-Completeness proof of the Coverage Problem that we have presented in [21], because coverage can be seen as a particularly simplified throughput problem using an on/off, SINR-threshold-based, throughput function.

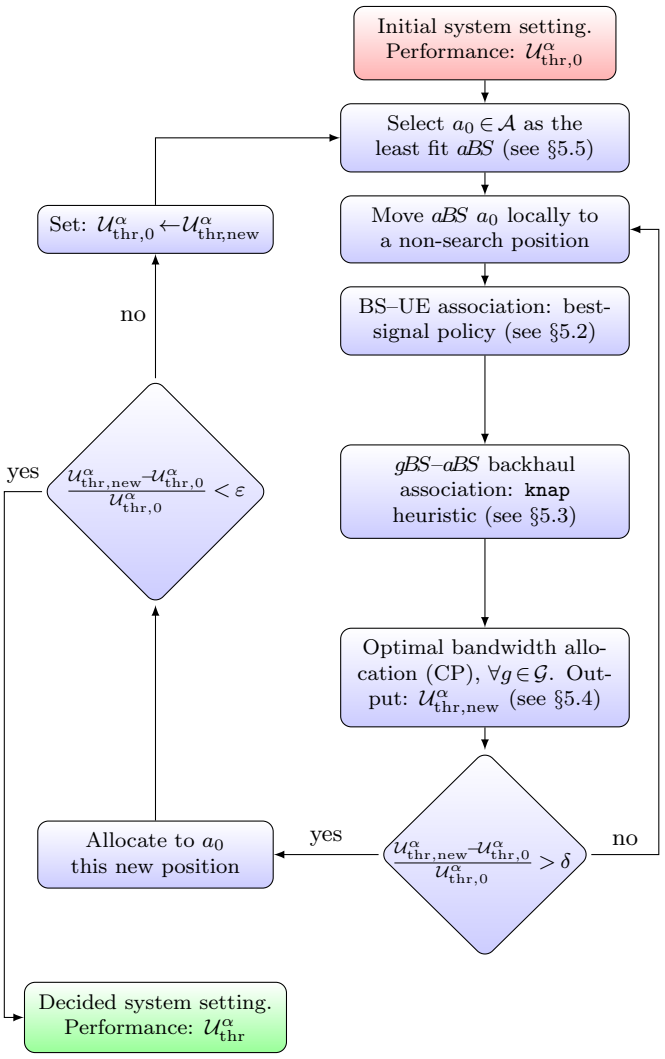


Figure 4: Flow diagram of PADD operation.

## 5. Extremal Optimization

The optimization framework proposed in Section 4 is non-convex and mixed-integer, hence not solvable with any off-the-shelf optimizer [49]. The problem is hard to solve because any change in a decision variable (e.g., a position of a drone) affects backhaul and user association, as well as interference and resource allocation for all users. Due to the intertwined nature of the decision variables of the problem, this is the kind of problems EO has been thought for.

To find time-efficient and near-optimal solutions, we propose a Parallelized Alfa-fair Drone Deployment (PADD) algorithm, based on a typical EO operation. We base the design of PADD on decoupling the problem in the four main decisions that the optimization framework must make: (*i*) the 3D positions of the fleet of *aBS*s; (*ii*) the sets of users attached to each *gBS* and *aBS*; (*iii*) *gBS*–*aBS* backhaul association; (*iv*) bandwidth allocation to backhaul links *gBS*–*aBS* as well as to access links from each *gBS* or *aBS* to their attached users.

In what follows, we formally describe the PADD operation and provide details of each step that PADD takes. The algorithm iteratively solves four steps, as pictured in Figure 4 as a flow-chart: after deriving an initial feasible system setting, the least fit *aBS* $a_0$ is selected in order to locally probe non-searched positions that improve the current network performance. While probed positions do not provide a relative improvement of $\delta \geq 0$ over the current network performance, new local non-searched positions are probed. In case a probed position improves performance, *aBS* $a_0$ is

$$\max_{B^{g,a}} U^{\alpha}_{\text{bhl}} = \begin{cases} \sum\limits_{g\in\mathcal{G}} \sum\limits_{a\in\mathcal{A}} \left( \frac{|\mathcal{U}_a|}{|\mathcal{U}_g \bigcup \mathcal{U}_a|} \log_2\left(1+\gamma^{\mathcal{B}}_{g,a}\right) \right)^{1-\alpha} \cdot \frac{B^{g,a}}{1-\alpha}, & \alpha \neq 1; \\ \sum\limits_{g\in\mathcal{G}} \sum\limits_{a\in\mathcal{A}} \log\left( \frac{|\mathcal{U}_a|}{|\mathcal{U}_g \bigcup \mathcal{U}_a|} \log_2\left(1+\gamma^{\mathcal{B}}_{g,a}\right) \right) \cdot B^{g,a}, & \alpha = 1; \end{cases}$$

s.t.:

$$\sum_{a\in\mathcal{A}} B^{g,a} \leq A_g, \qquad \forall g \in \mathcal{G};$$

$$\sum_{g\in\mathcal{G}} B^{g,a} = 1, \qquad \forall a \in \mathcal{A}.$$

Figure 5: Backhaul Association Optimization Program.

*moved* to such position and the current system performance is updated. In case this new performance provides a relative improvement higher than $\varepsilon \geq \delta$, the new least fit *aBS* is selected and the process begins again. Otherwise, the algorithm converges and outputs the decided system setting. Specifically, the convergence of PADD is guaranteed because the algorithm only accepts new system configurations if the utility improves by at least $\varepsilon > 0$, and stops otherwise. Since the utility is bounded by the value reached at the optimum, which is a finite value obtained as a finite sum of finite quantities, our algorithm cannot keep upgrading the utility by a constant improvement of $\varepsilon$ indefinitely, so that PADD eventually must converge. We next formalize the operation of PADD more in detail.

### *5.1. Initial System Setting*

Initially, we consider a naive drone positioning. For instance, any random placement of drones provides a feasible solution that could be iteratively improved. However, we more efficiently select those locations that are closer to *gBS*s–so to guarantee good backhaul links–and those locations that are above densely populated regions–which are regions that potentially need drone relay assistance. This initial drone setting yields utility $U^{\alpha}_{\text{thr},0}$. However, in order to compute $U^{\alpha}_{\text{thr},0}$, we need to know also user association, backhaul association and resource allocation. These decisions are made as described in the following subsections.

### *5.2. BS–UE Association: Best-Signal Policy*

For fixed positions of the drones, the BS–UE association is performed individually by each user according to the best-signal policy described in Section 3.3, which is at most linear in the number of base stations $|\mathcal{B}|$, with $\mathcal{B} = \mathcal{G} \cup \mathcal{A}$. However, before association, we need to compute $|\mathcal{B}|$ SNR values for each UEs, and sort them in decreasing order, which goes with $|\mathcal{B}| \log |\mathcal{B}|$. The complexity of user association is therefore $\mathcal{O}(|\mathcal{B}| \log |\mathcal{B}|)$ comparisons, for each user.

In the following, the set of users attached to a *gBS* $g \in \mathcal{G}$ and the set of users attached to an *aBS* $a \in \mathcal{A}$ are denoted as $\mathcal{U}_g$ and $\mathcal{U}_a$, respectively.

### *5.3. **gBS–aBS** Backhaul Association: `GAP-Knap` Heuristic*

For fixed drone positions and given BS–UE association, the backhaul association is solved by assuming that the bandwidth $W_{\mathcal{G}}$ is proportionally shared among users connected to a *gBS* and to the *aBS*s to be connected to that *gBS*.

Specifically, the backhaul throughput is computed with the Shannon formula, using a fraction of bandwidth proportional to the number of users attached to the drone, and with the SINR resulting from current position of drone and the fixed position of *gBS*. Maximizing the $\alpha$-fairness of such throughput values for all drones, translates into a generalized assignment problem (GAP) [50]. With the notation used in Figure 3, in which $\gamma^{\mathcal{B}}_{g,a}$ is the backhaul SINR of link $(b, a)$ and $B^{g,a}$ denotes the binary decision variable that tells wether *gBS* $g$ associates with *aBS* $a$, we show the backhaul association optimization in Figure 5.

The first constraint states that each *gBS* can provide backhaul service to at most $A_g$ *aBS*s. The second constraint states that each *aBS* $a$ must be associated with one *gBS*.

$$\max_{w^a, w_u, T_u} U^{\alpha}_{\text{cvx},g} = \begin{cases} \sum\limits_{u \in \bigcup\limits_{b \in \mathcal{B}_g} \mathcal{U}_b} (T_u)^{1-\alpha} \cdot \frac{1}{1-\alpha}, & \alpha \neq 1; \\ \sum\limits_{u \in \bigcup\limits_{b \in \mathcal{B}_g} \mathcal{U}_b} \log(T_u), & \alpha = 1; \end{cases}$$

s.t.:

$$w^a \geq W^{\min}_{\mathcal{B}}, \qquad \forall a \in \mathcal{A}_g;$$

$$\sum_{a \in \mathcal{A}_g} w^a = W_{\mathcal{B}};$$

$$T^a \leq w^a \log_2\left(1+\gamma^{\mathcal{B}}_{g,a}\right), \qquad \forall a \in \mathcal{A}_g;$$

$$w_u \geq W^{\min}_{\mathcal{G}}, \qquad \forall u \in \mathcal{U}_g;$$

$$\sum_{u \in \mathcal{U}_g} w_u = W_{\mathcal{G}};$$

$$w_u \geq W^{\min}_{\mathcal{A}}, \qquad \forall u \in \bigcup_{a \in \mathcal{A}_g} \mathcal{U}_a;$$

$$\sum_{u \in \mathcal{U}_a} w_u = W_{\mathcal{A}}, \qquad \forall a \in \mathcal{A}_g;$$

$$T_u \leq w_u \log_2(1+\gamma_{b,u}), \qquad \forall (b,u) \in \mathcal{B}_g \times \bigcup_{b' \in \mathcal{B}_g} \mathcal{U}_{b'} \mid u \in \mathcal{U}_b;$$

$$\sum_{u \in \mathcal{U}_a} T_u \leq T^a, \qquad \forall a \in \mathcal{A}_g;$$

$$\sum_{u \in \mathcal{U}_g} T_u + \sum_{a \in \mathcal{A}_g} T^a \leq \tau_g.$$

Figure 6: Bandwidth Allocation Optimization Program.

GAP is an NP-hard MILP [51]. Hence, although the GAPs that PADD needs to solve have a small size and could be optimally solved by means of standard methods as a Branch&Bound search [52], such an approach would not lead to a polynomial-time algorithm. Hence, multiple heuristics have been proposed in literature to find near-optimal solutions to the GAP [53, 51]. In particular, we perform a simple heuristic based on an approximation to the 0-1 knapsack problem [54] by means of dynamic programming [55]. The resulting heuristic results into a 2-approximation heuristic [51], and hence its performance is theoretically bounded (although, in practice, we have observed an average approximation factor of 1.0021 and of 1.0222 in the worst case, hence showing a near-optimal performance). We name this heuristic as `GAP-knap`, which has a polynomial complexity of $\mathcal{O}(|\mathcal{G}| \cdot |\mathcal{A}| \cdot A_g)$. The complexity of `GAP-knap` is linear with the sizes of $\mathcal{G}$ and $\mathcal{A}$ and the maximum number of *aBS*s allowed to attached to *gBS*s, $A_g$.

### *5.4. Optimal Bandwidth Allocation: Convex Program*

For fixed drone positions, BS–UE association and *gBS*–*aBS* backhaul association, the optimal bandwidth allocation is solved by each *gBS* in parallel, with a convex program.

Each *gBS* must perform bandwidth allocation to split backhaul resources among the served *aBS*s, split *gBS*–UE access resources among the attached users $\mathcal{U}_g$, and the attached *aBS*s $a$ must split *aBS*–UE access resources among the users attached to each *aBS* $a$, $\mathcal{U}_a$. Since all these bandwidth allocations are intertwined (*aBS*–UE allocation depends on the backhaul bottleneck, *gBS*–*aBS* allocation depends on the number of attached *aBS*s to the same *gBS* and the number of final users of each *aBS*, and *gBS*–UE access resources depend also on the backbone service that the *gBS* gets from the internet), we formulate the bandwidth allocation optimization as a convex program in Figure 6.

In the program, $w^a$ is the share of total bandwidth that *gBS* $g$ allocates to *aBS* $a$, $T^a$ is the backhaul throughput for *aBS* $a$, $w_u$ is the share bandwidth that BS $b$ allocates to user $u$, and $T_u$ is the access service throughput for user $u$. $\mathcal{A}_g$ is the set of *aBS*s attached to *gBS* $g$, and $\mathcal{B}_g = \{g\} \cup \mathcal{A}_g$ is the set of *gBS* $g$ jointly with $\mathcal{A}_g$. $U^{\alpha}_{\text{cvx},g}$ is the utility function of *gBS* $g$, which is based on the $\alpha$-fairness metric.

The problem is convex, hence it is optimally solvable in polynomial time by means of standard interior-point methods [56]. However, these methods run in cubic time with respect to the number of users, i.e., the complexity is $\mathcal{O}(|\mathcal{U}|^3)$ [57]. This cubic complexity might soon become prohibitive for real-time applications such as drone-aiding and

fast repositioning in wireless networks (especially for big populations), as addressed in this article. Nevertheless, our convex problem can be analytically solved, as we show in a more comprehensive technical report addressing various aspects of throughput optimization with drone coverage [58]. In there, we apply KKT conditions [59] and show that finding the exact solution for each *gBS* $g$ is linear with respect to the number of users and *aBS*s attached to *gBS* $g$, i.e., $\mathcal{O}(U_{\max} \cdot A_g)$.

### 5.5. Least Fit Drone Selection

PADD iteratively improves the utility until convergence. The algorithm uses the idea behind EO algorithms. It selects the *least fit* element and re-sets its parameters in order to improve system performance. In our case, an *aBS* is selected and a new location is *probed*.

The choice of which *aBS* is the least fit is made based on the consideration that there are two factors that cause sub-optimality of *aBS* positions: (i) the *aBS* has a bad backhaul connectivity, hence it provides a worse service to users than what the access channel conditions allow, i.e., access resources are wasted; or (ii) the *aBS* offers bad access connectivity to users due to inter-drone interference, even though it has a good backhaul service, so that backhaul resources are wasted. Accordingly, we derive two indicators of sub-optimality as the relative difference between the aggregate utility from *aBS*-served users (namely $U^{\alpha}_{\text{thr},a}$) and the following quantities: (i) the utility of the *aBS* assuming infinite backhaul capacity, namely $U^{\alpha,B_\infty}_{\text{thr},a}$; and (ii) the utility of the *aBS* assuming no inter-drone interference, namely $U^{\alpha,SNR}_{\text{thr},a}$. Eventually, we pick as least fit *aBS* the drone $a_0$ that provides the higher value of all sub-optimality indicators:

$$a_0 = \arg\max_{a \in \mathcal{A}} \left( \max \left( \left| \frac{U^{\alpha,B_\infty}_{\text{thr},a} - U^{\alpha}_{\text{thr},a}}{U^{\alpha,B_\infty}_{\text{thr},a}} \right|, \left| \frac{U^{\alpha,SNR}_{\text{thr},a} - U^{\alpha}_{\text{thr},a}}{U^{\alpha,SNR}_{\text{thr},a}} \right| \right) \right). \tag{1}$$

Computing utilities for *aBS* $a$ needs $\mathcal{O}(U_{\max})$ sums and powers (logarithms for $\alpha = 1$). Hence, finding the maximum shown in Eq. (1) has complexity $\mathcal{O}(|\mathcal{A}| \cdot U_{\max})$ powers (or logarithms), the sums incurring negligible extra complexity.

Having identified $a_0$, PADD selects a new random position within the allowed 3D ball space around the current position of the drone.

### 5.6. Complexity of PADD

In this section we provide the complexity of PADD. The algorithm consists of sequential steps, involving: user association with BSs; the backhaul association solved with the GAP problem of Figure 5; the resource allocation of each *gBS* solved with the convex optimization of Figure 6; the system utility evaluation with the $\alpha$-fairness metric; and the least fit drone selection of the EO operation. Specifically, at each iteration, we have:

**Step 1** *User association.* This can be implemented on parallel threads: one thread per UE ranks the candidate list of BSs to attach to, then a separate thread computes the association in at most as many rounds as the number of BSs, as seen in Section 5.2. With $|\mathcal{U}|$ parallel threads, the complexity required for this step to rank the list of BSs is $\mathcal{O}\left(\frac{1}{2\log 2}|\mathcal{B}| \log |\mathcal{B}|\right)$ sums and comparisons.

**Step 2** *Backhaul association.* The next step consists in solving the `GAP-knap` problem for backhaul association, which must be done with a single thread, as shown in Section 5.3. The complexity of combining dynamic programming and the knapsack problem to solve this step is analyzed in [50] and it is $\mathcal{O}\left(2A_g|\mathcal{G}||\mathcal{A}|\right)$ sums or comparisons.

**Step 3** *Resource allocation.* This requires a thread per each *gBS* for which we need to solve the convex problem of Figure 6, as shown in Section 5.4. The time needed to complete this step is therefore the time needed to solve a single problem. In [58], it can be found an exhaustive and detailed solution to this single convex optimization problem in an exact way. Hence, here we remark that the complexity of the costliest case is $\mathcal{O}\left(4A_g U_{\max}\right)$ simple operations (e.g., sums), as discussed in [58].


Figure 7: Topology of Leganés (Spain) and *gBS*s placement.

**Step 4** *Utility evaluation.* The current configuration is evaluated in terms of $\alpha$-fair utility, which has the cost of $|\mathcal{U}||\mathcal{B}|$ sums or comparisons (for $\alpha \to \infty$) plus $|\mathcal{B}|$ power operations (for $\alpha \neq 0, 1$) or logarithms (for $\alpha = 1$). As discussed at the beginning of this section and depicted in Figure 4, the current configuration can be discarded and a new position is probed for the current least fit drone (back to **Step 1**).[1]

**Step 5** *Least fit selection.* Eventually, the algorithm computes the least fit drone with a single thread, with complexity $\mathcal{O}(4|\mathcal{A}|U_{\max})$ operations, as two kinds of additional different utilities need to be computed in Eq. (1) of Section 5.5.

As a result, the overall PADD's complexity is $\mathcal{O}\Big(N\Big(\frac{0.5}{\log 2}|\mathcal{B}|\log|\mathcal{B}|+2A_g|\mathcal{G}||\mathcal{A}|+4A_gU_{\max}+|\mathcal{U}||\mathcal{B}|\Big)\Big)$ simple operations (e.g., sums or comparisons) and $\mathcal{O}\left(N|\mathcal{B}|+4|\mathcal{A}|U_{\max}\right)$ complex operations (e.g., powers or logarithms). This means that PADD's complexity is low-order polynomial, linear with respect to the number of mobile users and log-linear with respect to the number of BSs.

Moreover, PADD's iterations converge very fast (we have observed no more than a hundred iterations) and our algorithm implemented on MATLAB took at most about 800 billion floating-point operations to optimize drone positions, which requires, e.g., about 10 s on a linux machine with an Intel Xeon E5-2670 processor at 2.6 GHz with a processor performing 32 flops/cycle with 64-bit operations.

## 6. Numerical Simulations

Here we present the numerical evaluation of the $\alpha$-fair cellular capacity optimization in both static and dynamic scenarios. All our simulations are performed over the real topology of an operational network deployed in a dense city: 150,000 inhabitants in a 10 km$^2$ area (Leganés, south of Madrid, Spain) [60]. The area is covered by 10 *gBS*s using the same LTE band, as shown in Figure 7.

As there are several operators in Spain providing LTE service over multiple bands, and we only consider one operator in one band, we use a number of 1000 UEs that request service at the same time, unless otherwise specified.

First, we numerically validate our proposed PADD in comparison with optimal results approximated by means of Monte-Carlo (MC) simulations in static networks with limited population: We perform $10^7$ MC runs per instance where *aBS*s are placed in feasible random positions. Then, we optimize the network for each run and save the best setting as the approximated optima. Second, we analyze the robustness of the system model in order to prove that assuming perfect knowledge about user positions has limited impact on performance. Eventually, we study three significant static and dynamic scenarios:

[1] When the optimization problem is initialized, there is no least fit drone yet; thus, the first iteration executes **Step 1**-**Step 4** only once, then it moves to **Step 5** to make the first least fit selection.

Table 3: Evaluation Parameters

| ***Parameter*** | ***Value*** |
|---|---|
| $\xi_{LoS}$, $\xi_{NLoS}$, $\beta_1$, $\beta_2$ | 1.6 dB, 23 dB, 12.08, 0.11 |
| Carrier frequencies, $f_{\mathcal{G}}$, $f_{\mathcal{A}}$ | 1815.1 MHz, 2.63 GHz |
| Bandwidths, $W_{\mathcal{G}}$, $W_{\mathcal{A}}$ | 18 MHz, 18 MHz |
| Tx power, $P^g_{Tx}$, $P^a_{Tx}$ | 44 dBm, 25 dBm |
| Thermal Noise Power | -174 dBm/Hz |
| Ground path loss exponent, $\eta_{BS}$ | 3 |
| Height range, $[h_{\min}, h_{\max}]$ | $[40, 300]$ m |
| Urban area, $\lvert\mathcal{S}\rvert$ | 10 km$^2$ |
| Average walking speed | 2.5 m/s |
| Monte-Carlo runs per instance | $10^7$ |
| Instances of simulations | 1000 |

- *Poisson Point Process (PPP)*: we statically place UEs on the city map according to a Poisson point process [61].
- *Stadium*: we statically place 60% of the UEs in the surroundings of a stadium, and the rest like in *PPP*.
- *Event*: 40% of the population of UEs moves according to the random way-point model, whereas other UEs keep arriving at an official scheduled rate of a train station and move towards the stadium.

For each scenario, we study drone placement, utility and throughput achieved, and system fairness measured with the Jain's index [62].

Table 3 reports the evaluation parameters used in our simulations. We take a carrier bandwidth of 20 MHz for both *gBS* and *aBS* channels (out of which, we consider that 10% is for guard bands, so we only use 18 MHz [47]). The carrier frequency of cellular links is 1815.1 MHz, while for air-to-ground links we use 2630 MHz. These are two commonly used LTE bands [60]. The transmission power of *aBS*s is 25 dBm, notably lower than the 44 dBm power transmission of the ground *gBS*s. In addition, probed aerial positions arise from a lattice that spans equal-volume subspaces.

To position our proposal, we consider the performance without drones as baseline (`Ground` in the figures). Moreover, to compare PADD to state of the art drone-position optimization frameworks, we have implemented and tested the *Repulsion-Attraction* scheme (`RA`) [63].

Although our analysis holds for generic values of $\alpha$, we present results for three specific and most interesting cases:

(i) For $\alpha = 0$, we obtain the maximum throughput achievable (`MaxThr` in the figures).

(ii) For $\alpha = 1$, we optimize the proportional fairness network metric (`PropFair` in the figures).

(iii) For $\alpha \to \infty$, we optimize the max-min fairness network metric (`MaxMin` in the figures).

We study these three metrics for the following reasons. The `MaxThr` metric provides the maximum achievable network capacity, without fairness. The `PropFair` metric takes into account the network capacity but it also does not let fairness decay. The mathematical design of this metric, which optimizes the aggregation of logarithms of user throughputs, allows for finding a trade-off between a high system capacity and high fairness values. The `MaxMin` metric only targets fairness of the weakest customer, which comes at the cost of providing lower aggregate throughput. Both the `PropFair` and `MaxMin` have been adopted in the implementation of real telecommunication systems [64] as well as in many research works [65, 66].

We have simulated every analyzed use-case 1000 times using MATLAB `R2020a` and show average results. Error bars in the figures are 95% confidence intervals.

### *6.1. Validation of PADD Operation*

Here we compare PADD results and optima (approximated by means of `MC`, since there are no computationally feasible alternatives) in the *PPP* scenario, and comment on the basic properties of our approach.

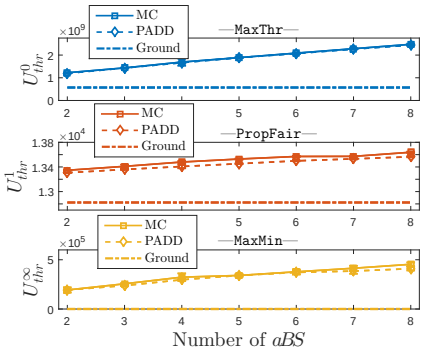


Figure 8: Utility validation for $\alpha \in \{0, 1, \infty\}$. $G = 10$, $U = 1000$. Scenario: *PPP*.

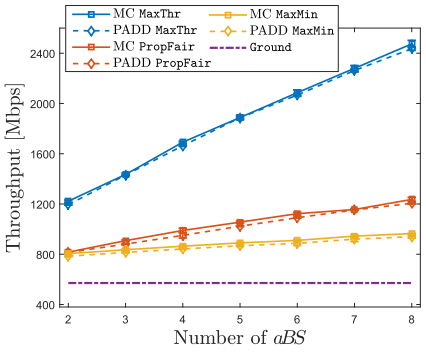


Figure 9: Network capacity validation for $\alpha \in \{0, 1, \infty\}$. $G = 10$, $U = 1000$. Scenario: *PPP*.

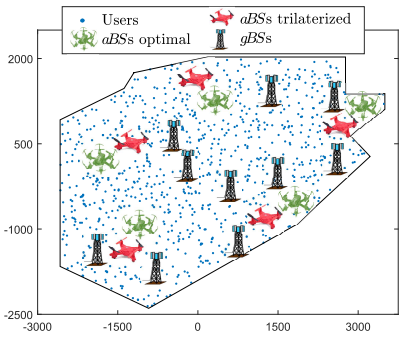


Figure 10: Robustness validation for $\alpha = 1$. *aBS*s placement error. $G = 10$, $A = 5$, $U = 1000$. Scenario: *PPP*.

In Figure 8, we present a utility comparison between the `Ground` scheme, optima results from `MC` and our proposal PADD with the three main metrics studied in this article (`MaxThr`, `PropFair` and `MaxMin`). Note that different values of $\alpha$ make utility values very different, so we cannot compare utilities across fairness metrics. So, we will compare PADD and the existing schemes on a per-metric basis.

We observe that the difference between utilities achieved with PADD and `MC` is negligible, below 1% in all cases. This shows that our proposal PADD is able to achieve close-to-optimal results with a much lower complexity. Furthermore, PADD matches very well also the throughput achievable in the optimal case, as illustrated in Figure 9. This shows that PADD is able to pursue the optimal system configuration, not just an operational configuration that is near-optimal according to the chosen utility metric.

The figures show that, in the PPP scenario, utility and throughput increase with fleet size. This is because user's density is homogeneous over the entire area, so that drones are spaced apart, and inter-drone interference constraints do not kick in. Note also that the gain in terms of utility and throughput with respect to the `Ground` configuration is remarkable under all considered metrics, which confirms that coordinated drone relays have huge potential.

### *6.2. Robustness of PADD*

In the system model described in Section 3, we have assumed that the positions of users are known. However, it might be not realistic to estimate user locations with negligible error unless GPS is enabled or many drones are available [67]. For instance, using a trilateration on the signal strength at the base station, the error on the position is normally below 50 m [68]. Hence, here we consider the PPP scenario to numerically analyze the robustness of PADD by introducing uncertainty in the position of the ground users, uniformly at random, within 50 m.

In Figure 10, we observe that the position of drones selected by PADD is similar with and without localization errors. Indeed, we have quantified an average utility relative loss below 5% (see Appendix B for further details). The reason of such robust behavior stands in the fact that the optimization of drone positions is done based on many users and in relatively large areas, so that multiple errors in user positions are not so important, whereas the presence of a distributed mass of users in a given area is what actually catalyzes the presence of a drone.

Next, we analyze non-homogeneous user topologies in static and dynamic cases.

### *6.3. Performance Evaluation in the Static Stadium Case*

The *Stadium* scenario allows to study network performance when the ground network cannot sustain the UE's demand.

In Figure 11 we show the average performance experienced by all users in the overall, city-wide, scenario, while in Figure 12 we focus on the performance of users in and nearby the stadium. We observe that PADD with `MaxThr` benefits of the presence of drones (see Figure 11, top), although adding drones is negative for users by the stadium (see

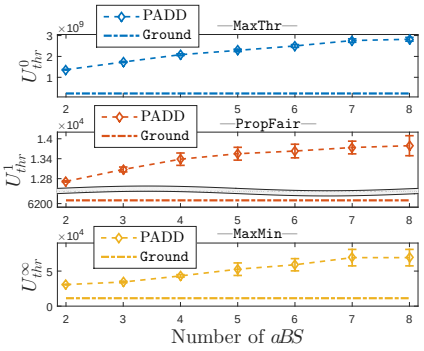


Figure 11: Utility of all users for $\alpha \in \{0, 1, \infty\}$. $G = 10$, $U = 1000$. Scenario: *Stadium* with $U_d = 600$.

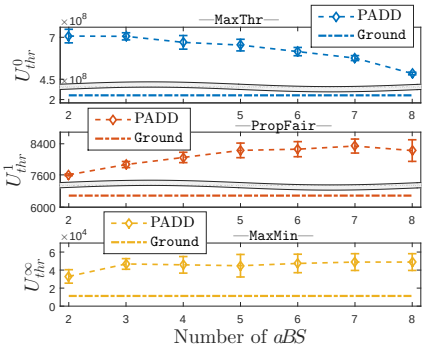


Figure 12: Utility of stadium users for $\alpha \in \{0, 1, \infty\}$. $G = 10$, $U = 1000$. Scenario: *Stadium* with $U_d = 600$.

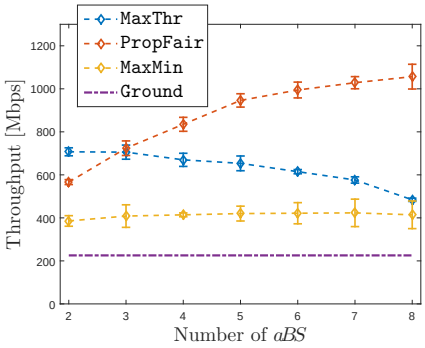


Figure 13: Throughput of stadium users for $\alpha \in \{0, 1, \infty\}$. $G = 10$, $U = 1000$. Scenario: *Stadium* with $U_d = 600$.

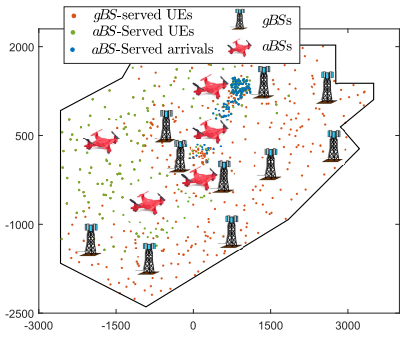


Figure 14: Network state at $t = 25$ min. $G = 10$, $A = 5$, $U = 640$. Scenario: `PropFair`, *Event*.

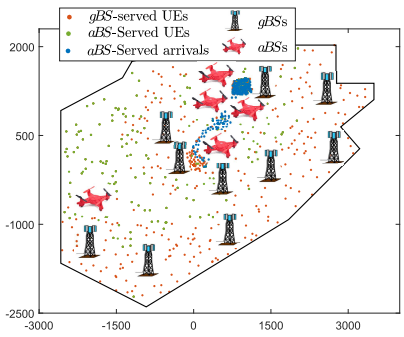


Figure 15: Network state at $t = 60$ min. $G = 10$, $A = 5$, $U = 880$. Scenario: `PropFair`, *Event*.

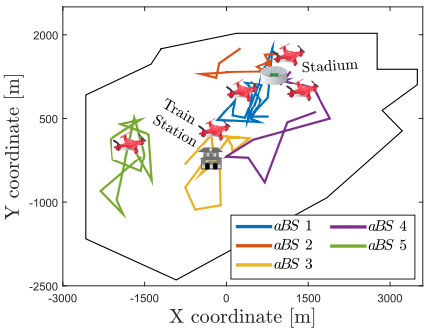


Figure 16: Drone trajectories during 75 minutes. $G = 10$, $A = 5$, $U = [400, \ldots, 1000]$. Scenario: `PropFair`, *Event*.

Figure 12, top). In fact, adding *aBS*s introduces more capacity and connectivity opportunities, hence the benefit at aggregate city level. However, PADD with `MaxThr` seeks for drone positions where they are less impaired by interference, so to generate a few good-quality channels. This behavior results into having only one or two *aBS*s at most located near the stadium. More *aBS*s would interfere too much. Hence, as long as *aBS*s are added, PADD with `MaxThr` positions them apart from the stadium, yet they generate some interference, which progressively worsens the performance of users by the stadium.

PADD with `PropFair` behaves completely different. It brings drones where it favors users otherwise served below the average, so to increase the system's log utility. This results in deploying *aBS*s by the stadium, where the density of users in the presence of limited radio resources hinders performance more than radio channel quality issues.

With `MaxMin`, PADD positions drones where users would otherwise suffer the worst connection quality, irrespective of their closeness to densely populated areas. Therefore the aggregated throughput is lower than with `PropFair`, which in turn is much lower than with `MaxThr`.

If we now consider only users by the stadium, Figure 13 illustrates how using `PropFair` can clearly outperform `MaxThr` in terms of throughput. This is due to the fact that the optimization of throughput requires positioning drones where they interfere less, which is not necessarily by the stadium. Indeed, due to interference, users by the stadium could incur a loss by increasing the number of drones even in the case of using `MaxMin`, as shown in the figure.

As a result of the previous numerical analysis, we observe that using *aBS*s can be beneficial to help the ground cellular network in dense spots, except it cannot help in purely maximizing throughput (e.g., with `MaxThr`). Drones cannot either "rescue" all users with bad channel conditions, as PADD would seek with `MaxMin` and `PropFair`. However, PADD can always provide fairness and large throughput gain with respect to the `Ground` case. Besides, the version of

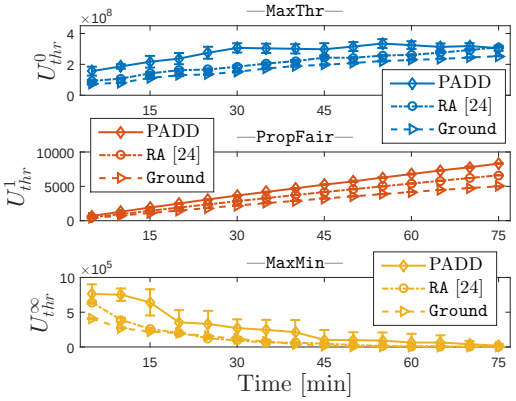


Figure 17: Attendance utility for $\alpha \in \{0, 1, \infty\}$. $G = 10$, $A = 5$, $U = [400, \ldots, 1000]$. Scenario: *Event*.

PADD with `PropFair` results to be quite effective in case of dense masses of users.

### *6.4. Performance Evaluation in the Dynamic Event Case*

The last scenario we consider is dynamic and allows us to study the evolution of network performance *while* the density of users increases. Moreover, it shows the importance of designing a fast and reactive algorithm to re-position drones as the user topology changes.

In the Event scenario, small masses of 40 users arrive periodically to the train station of the city every 5 minutes. The initial population is 400 users and keeps growing during 75 minutes up to 1000 users. There are 5 *aBS*s hovering the area in this example. Upon a train arrival, the new mobile users walk towards the stadium, located 1.5 km away from the train station. The fleet is repositioned every 5 simulated minutes, using as initial condition the positions of the 5 drones in the previous optimization epoch.

We first illustrate how the network evolves over time in Figs. 14 and 15, using PADD with `PropFair`. After 25 minutes (Figure 14) some people are already at the stadium, while many others keep arriving and are walk towards it. At that point in time, 3 *aBS*s are getting prepared to serve the users nearby the stadium and also the smaller groups on their way from the train station to the stadium. We see how drones adapt their positions after other 35 minutes, in Figure 15, when much more users have reached the stadium. By that time, one more drone has been dispatched as well, to serve the stadium. The trajectories of the drones for a 75-minute simulation instance are shown in Figure 16, where the red drones represent the source position of *aBS*s. In the figure, we can see that *aBS* 5 is not required to assist the dense stadium spot, while *aBS*s 1 and 2 are always hovering between the train station and the stadium. Also, *aBS*s 3 and 4 keep moving back and forth within different regions, to fairly supply the demand of users.

As concerns performance, Figure 17 illustrates utility as it evolves over time. Here, in addition to PADD with the three selected values of $\alpha$, we also compare the *Repulsion-Attraction* (`RA`) scheme. With `RA`, *aBS*s are attracted by UE's inverse SNR, and repulsed by proximity to *gBS*s to avoid interference. `RA` does not target any fairness metric, so we quantify its impact with the same utility functions used for PADD computed for users arriving over time (the *attendance*).

As time passes by, and more people reach the stadium, Figure 17 shows a significant utility raise under the adoption of either `MaxThr` or `PropFair` schemes. With `MaxThr`, the gain of PADD over `RA` and `Ground` schemes is high, although it saturates quickly. Instead, with `PropFair`, PADD exhibits a smoother behavior, as its gain keeps increasing.

Under the `MaxMin` scheme, PADD performs better than `RA`, although now we observe a decay of performance over time, for all schemes. This is due to the fact that, with more attendance, the minimum per-user achieved rate will have to decrease, unless more drones where deployed.

Clearly, the `RA` scheme is not able to opportunistically take advantage of user's diversity and improve utility because it does not target a throughput-based metric, unlike PADD. This permits PADD to optimize the network with much better guarantees in terms of throughput and fairness.

## 7. Lessons learnt and discussion

The performance assessment carried in this article shows the importance of integrating a fleet of drone relay stations in a cellular network. It also unveils that optimizing drone positions to maximize throughput, without taking into account fairness, has little relevance in the presence of dense spots or ground users. Instead, a fair metric like `PropFair` provides notable throughput and utility improvements.

The fact that PADD is fast, allows to design an almost continuous reconfiguration of positions in realistic networks, as shown in this article. In turn, our scheme is fast because we have designed it by segmenting the problem into a few phases: we use EO for optimizing drone positions, while wireless backhaul attachment, BS selection and distributed resource allocation are sequentially solved optimally and analytically for each drone deployment topology.

The actual implementation of PADD requires the exchange of signaling information between drones and a centralized orchestrator, as well as the implementation of a mechanism to track users. Signaling incurs some limited overhead to instruct drones and to gather user positions and interference reports (which are however already collected by current BSs), depending on the frequency of reconfigurations. However, we have seen that PADD is robust to imprecise tracking of user's positions, which can be therefore strongly simplified, so that the additional overhead due to PADD will mostly be due to controlling drones.

Finally, we comment on drone mechanicals. Current commercial drones can carry small BSs and access points, although they cannot fly for long time due to battery limitations (around 30 minutes at most). They can easily move at the reasonable speed of 15 m/s. Therefore, it is possible to derive a repositioning scheme that accounts for replacing drones that go back to the charging station if the drones do not fly too far from it. For the case considered in Section 6.4, the routes flown by drones in 5 minutes are short enough, and it is easy to hover a city district in a few minutes. Thus, notwithstanding the intricacies of the analysis, the performance evaluation discussed in this article is quite relevant for realistic systems.

## 8. Conclusions

In this article we have proposed an analytic framework to optimize drone-aided cellular networks in terms of an $\alpha$-fair throughput utility function, under realistic stochastic models. Specifically, we have studied the integration of a coordinated fleet of *aerial base stations* carried by drones and relaying traffic for ground base stations by means of 3D-beamforming wireless backhaul connections. Due to the complexity of the studied problem, we have proposed PADD, an optimization algorithm based on extremal optimization that works in parallel threads. PADD provides near-optimal solutions in low-degree polynomial time, with a linear dependency on all parameters but for the number of base stations, which causes a sub-quadratic dependency. This makes PADD suitable for implementation in dynamically changing environments. The performance evaluation presented in the article shows that PADD brings significant gain and outperforms existing approaches. It also unveils that using fairness is key to get benefit from coordinated yet interfering drone relay stations.

## Acknowledgment

The work of E. Arribas was partially supported by the FPU15/02051 grant from the Spanish Ministry of Education, Culture and Sports (MECD). The work of V. Mancuso was partially supported by the Spanish Ministry of Science and Innovation grant PID2019-109805RB-I00 (ECID) and by the Regional Government of Madrid and the European Union

through the European Regional Development Fund (ERDF) as part of the response from the European Union to the COVID-19 pandemic in the context of REACT-CONTACT-CM-23479 research project.

## References

[1] E. Arribas, V. Mancuso, V. Cholvi, Fair cellular throughput optimization with the aid of coordinated drones, in: IEEE Conference on Computer Communications Workshops (INFOCOM WKSHPS), IEEE, 2019, pp. 295–300.

[2] W. Mohr, 5G empowering vertical industries, in: Tech. Rep., 5G PPP, 2016.

[3] M. Maternia, et al., 5G PPP use cases and performance evaluation models, in: Tech. Rep., 2016.

[4] C. Liu, K. Sundaresan, M. Jiang, S. Rangarajan, G.-K. Chang, The case for re-configurable backhaul in cloud-RAN based small cell networks, in: IEEE Conference on Computer Communications (INFOCOM), IEEE, 2013, pp. 1124–1132.

[5] V. Genc, S. Murphy, J. Murphy, Performance analysis of transparent relays in 802.16j MMR networks, in: International Symposium on Modeling and Optimization in Mobile, Ad Hoc, and Wireless Networks and Workshops (WiOpt), IEEE, 2008, pp. 273–281.

[6] I. Bor-Yaliniz, H. Yanikomeroglu, The new frontier in RAN heterogeneity: Multi-tier drone-cells, IEEE Communications Magazine 54 (11) (2016) 48–55.

[7] W. Guo, C. Devine, S. Wang, Performance analysis of micro unmanned airborne communication relays for cellular networks, in: International Symposium on Communication Systems, Networks & Digital Sign (CSNDSP), IEEE, 2014, pp. 658–663.

[8] W. Guo, T. O'Farrell, Relay deployment in cellular networks: Planning and optimization, IEEE Journal on Selected areas in Communications 31 (8) (2012) 1597–1606.

[9] M. Mozaffari, W. Saad, M. Bennis, M. Debbah, Wireless communication using unmanned aerial vehicles (UAVs): Optimal transport theory for hover time optimization, IEEE Transactions on Wireless Communications 16 (12) (2017) 8052–8066.

[10] J. Mo, J. Walrand, Fair end-to-end window-based congestion control, IEEE/ACM Transactions on Networking 8 (5) (2000) 556–567.

[11] T. Lan, D. Kao, M. Chiang, A. Sabharwal, An axiomatic theory of fairness in network resource allocation, in: IEEE Conference on Computer Communications (INFOCOM), IEEE, 2010, pp. 1–9.

[12] S. Boettcher, A. Percus, Optimization with extremal dynamics, Physical Review Letters 86 (2001) 5211–5214.

[13] R. Ferrús, H. Koumaras, O. Sallent, G. Agapiou, T. Rasheed, M.-A. Kourtis, C. Boustie, P. Gélard, T. Ahmed, SDN/NFV-enabled satellite communications networks: Opportunities, scenarios and challenges, Physical Communication 18 (2016) 95–112.

[14] R. De Gaudenzi, M. Luise, L. Sanguinetti, The open challenge of integrating satellites into (beyond-) 5G cellular networks, IEEE Network 36 (2) (2022) 168–174.

[15] E. Arribas, V. Mancuso, Multi-path D2D leads to satisfaction, in: A World of Wireless, Mobile and Multimedia Networks (WoWMoM), IEEE, 2017, pp. 1–7.

[16] E. Arribas, V. Mancuso, Achieving per-flow satisfaction with multi-path D2D, Ad Hoc Networks 106 (2020) 102162.

[17] P. S. Bithas, V. Nikolaidis, A. G. Kanatas, G. K. Karagiannidis, UAV-to-ground communications: Channel modeling and UAV selection, IEEE Transactions on Communications 68 (8) (2020) 5135–5144.

[18] M. Mozaffari, W. Saad, M. Bennis, Y.-H. Nam, M. Debbah, A tutorial on UAVs for wireless networks: Applications, challenges, and open problems, IEEE Communications Surveys & Tutorials 21 (3) (2019) 2334–2360.

[19] I. Strumberger, M. Sarac, D. Markovic, N. Bacanin, Moth search algorithm for drone placement problem, International Journal of Computers 3 (2018).

[20] M. Mozaffari, W. Saad, M. Bennis, M. Debbah, Unmanned aerial vehicle with underlaid device-to-device communications: Performance and tradeoffs, IEEE Transactions on Wireless Communications 15 (6) (2016) 3949–3963.

[21] E. Arribas, V. Mancuso, V. Cholvi, Coverage optimization with a dynamic network of drone relays, IEEE Transactions on Mobile Computing 19 (10) (2019) 2278–2298.

[22] N. Kumar, M. Ghosh, C. Singhal, UAV network for surveillance of inaccessible regions with zero blind spots, in: IEEE Conference on Computer Communications Workshops (INFOCOM WKSHPS), IEEE, 2020, pp. 1213–1218.

[23] X. Liu, Y. Liu, Y. Chen, Reinforcement learning in multiple-UAV networks: Deployment and movement design, IEEE Transactions on Vehicular Technology 68 (8) (2019) 8036–8049.

[24] J. Cui, Y. Liu, Z. Ding, P. Fan, A. Nallanathan, QoE-based resource allocation for multi-cell NOMA networks, IEEE Transactions on Wireless Communications 17 (9) (2018) 6160–6176.

[25] B. Galkin, J. Kibiłda, L. A. DaSilva, A stochastic model for UAV networks positioned above demand hotspots in urban environments, IEEE Transactions on Vehicular Technology 68 (7) (2019) 6985–6996.

[26] D. Popescu, P. Jacquet, B. Mans, Connecting flying backhauls of unmanned aerial vehicles to enhance vehicular networks with fixed 5G NR infrastructure, IET Smart Cities (2022) 1-16.

[27] A. Alsharoa, H. Ghazzai, A. Kadri, A. E. Kamal, Spatial and temporal management of cellular HetNets with multiple solar powered drones, IEEE Transactions on Mobile Computing 19 (4) (2019) 954–968.

[28] M. Hua, L. Yang, C. Li, Q. Wu, A. L. Swindlehurst, Throughput maximization for UAV-aided backscatter communication networks, IEEE Transactions on Communications 68 (2) (2019) 1254–1270.

[29] X. Wang, X. Liu, J. Wu, W. Ju, X. Chen, L. Shen, Joint user scheduling, power configuration and trajectory planning strategy for UAV-aided WSNs, ACM Transactions on Sensor Networks.

[30] Y. Liang, L. Xiao, D. Yang, Y. Liu, T. Zhang, Joint trajectory and resource optimization for UAV-aided two-way relay networks, IEEE Transactions on Vehicular Technology 71 (1) (2021) 639–652.

[31] S. Mignardi, R. Marini, R. Verdone, C. Buratti, On the performance of a UAV-aided wireless network based on NB-IoT, Drones 5 (3) (2021) 94.

[32] S. Yin, F. R. Yu, Resource allocation and trajectory design in UAV-aided cellular networks based on multiagent reinforcement learning, IEEE Internet of Things Journal 9 (4) (2021) 2933–2943.

[33] J. Liu, H. Zhang, Y. He, Deployment optimization of UAV-aided networks through a dynamic tunable model, IEEE Communications Letters 25 (7) (2021) 2348–2352.

[34] L. Chiaraviglio, F. D'Andreagiovanni, W. Liu, J. A. Gutierrez, N. Blefari-Melazzi, K.-K. R. Choo, M.-S. Alouini, Multi-area throughput and energy optimization of UAV-aided cellular networks powered by solar panels and grid, IEEE Transactions on Mobile Computing 20 (7) (2020) 2427–2444.

[35] S. Iranmanesh, F. S. Abkenar, R. Raad, A. Jamalipour, Improving throughput of 5G cellular networks via 3D placement optimization of logistics drones, IEEE Transactions on Vehicular Technology 70 (2) (2021) 1448–1460.

[36] H. Shakhatreh, A. Alenezi, A. Sawalmeh, M. Almutiry, W. Malkawi, Efficient placement of an aerial relay drone for throughput maximization, Wireless Communications and Mobile Computing 2021.

[37] K. Ali, H. X. Nguyen, Q.-T. Vien, P. Shah, M. Raza, Deployment of drone-based small cells for public safety communication system, IEEE Systems Journal 14 (2) (2020) 2882–2891.

[38] D. Zhai, H. Li, X. Tang, R. Zhang, H. Cao, Joint position optimization, user association, and resource allocation for load balancing in uav-assisted wireless networks, Digital Communications and Networks (2022) In Press.

[39] G. Chen, X. B. Zhai, C. Li, Joint optimization of trajectory and user association via reinforcement learning for UAV-aided data collection in wireless networks, IEEE Transactions on Wireless Communications (2022) In Press.

[40] B. Danila, Y. Yu, J. A. Marsh, K. E. Bassler, Optimal transport on complex networks, Physical Review E 74 (4) (2006) 046106.

[41] A. BenMimoune, M. Kadoch, Relay technology for 5G networks and IoT applications, in: Internet of Things: Novel Advances and Envisioned Applications, Springer, 2017, pp. 3–26.

[42] Y. Zeng, J. Lyu, R. Zhang, Cellular-connected UAV: Potential, challenges, and promising technologies, IEEE Wireless Communications 26 (1) (2018) 120–127.

[43] E. Arribas, V. Cholvi, V. Mancuso, An optimal scheme to recharge communication drones, in: IEEE Global Communications Conference (GLOBECOM), IEEE, 2021, pp. 1–6.

[44] A. Al-Hourani, S. Kandeepan, A. Jamalipour, Modeling air-to-ground path loss for low altitude platforms in urban environments, in: IEEE Global Communications Conference (GLOBECOM), IEEE, 2014, pp. 2898–2904.

[45] A. Al-Hourani, S. Kandeepan, S. Lardner, Optimal LAP altitude for maximum coverage, IEEE Wireless Communications Letters 3 (6) (2014) 569–572.

[46] J. Goldhirsh, W. J. Vogel, Handbook of propagation effects for vehicular and personal mobile satellite systems, NASA Reference Publication 1274 (1998) 40–67.

[47] S. Sesia, I. Toufik, M. Baker, LTE-the UMTS long term evolution: From theory to practice, John Wiley & Sons, 2011.

[48] G. Das, R. Fraser, A. López-Ortiz, B. Nickerson, On the discrete unit disk cover problem, International Journal of Computational Geometry & Applications 22 (05) (2012) 407–419.

[49] S. Burer, A. N. Letchford, Non-convex mixed-integer nonlinear programming: A survey, Surveys in Operations Research and Management Science 17 (2) (2012) 97–106.

[50] M. L. Fisher, R. Jaikumar, L. N. Van Wassenhove, A multiplier adjustment method for the generalized assignment problem, Management Science 32 (9) (1986) 1095–1103.

[51] R. Cohen, L. Katzir, D. Raz, An efficient approximation for the generalized assignment problem, Information Processing Letters 100 (4) (2006) 162–166.

[52] W. Sun, Y.-X. Yuan, Optimization theory and methods: Nonlinear programming, Vol. 1, Springer Science & Business Media, 2006.

[53] D. G. Cattrysse, L. N. Van Wassenhove, A survey of algorithms for the generalized assignment problem, European journal of operational research 60 (3) (1992) 260–272.

[54] A. Fréville, The multidimensional 0–1 knapsack problem: An overview, European Journal of Operational Research 155 (1) (2004) 1–21.

[55] R. Andonov, V. Poirriez, S. Rajopadhye, Unbounded knapsack problem: Dynamic programming revisited, European Journal of Operational Research 123 (2) (2000) 394–407.

[56] Y. Nesterov, A. Nemirovskii, Interior-point polynomial algorithms in convex programming, Vol. 13, Siam, 1994.

[57] S. Bubeck, et al., Convex optimization: Algorithms and complexity, Foundations and Trends® in Machine Learning 8 (3-4) (2015) 231–357.

[58] E. Arribas, V. Mancuso, V. Cholvi, Fair throughput optimization with a dynamic network of drone relays, arXiv preprint arXiv: 2207.04955 (2022).

[59] H. Kuhn, A. Tucker, Nonlinear programming, in: Traces and Emergence of Nonlinear Programming, Springer, 2014, pp. 247–258.

[60] Ministerio de Asuntos Económicos y Transformación Digital de España, Niveles de exposición.
URL `https://geoportal.minetur.gob.es/VCTEL/vcne.do`

[61] G. Last, M. Penrose, Lectures on the Poisson process, Vol. 7, Cambridge University Press, 2017.

[62] R. K. Jain, D.-M. W. Chiu, W. R. Hawe, et al., A quantitative measure of fairness and discrimination, Eastern Research Laboratory, Digital Equipment Corporation, Hudson, MA 21 (1984).

[63] O. Andryeyev, A. Mitschele-Thiel, Increasing the cellular network capacity using self-organized aerial base stations, in: ACM Workshop on Micro Aerial Vehicle Networks, Systems, and Applications, ACM, 2017, pp. 37–42.

[64] G. Miao, J. Zander, K. W. Sung, S. B. Slimane, Fundamentals of mobile data networks, Cambridge University Press, 2016.

[65] S. Mosleh, L. Liu, J. Zhang, Proportional-fair resource allocation for coordinated multi-point transmission in LTE-advanced, IEEE Transactions on Wireless Communications 15 (8) (2016) 5355–5367.

[66] R. Li, P. Patras, Max-min fair resource allocation in millimetre-wave backhauls, IEEE Transactions on Mobile Computing 19 (8) (2019) 1879–1895.

[67] R. Petrolo, Y. Lin, E. Knightly, ASTRO: Autonomous, sensing, and tetherless networked drones, in: ACM Workshop on Micro Aerial Vehicle Networks, Systems, and Applications, ACM, 2018, pp. 1–6.

[68] J. A. del Peral-Rosado, R. Raulefs, J. A. López-Salcedo, G. Seco-Granados, Survey of cellular mobile radio localization methods: From 1G to 5G, IEEE Communications Surveys & Tutorials 20 (2) (2017) 1124–1148.

[69] R. P. Series, Propagation data and prediction methods required for the design of terrestrial line-of-sight systems, Recommendation ITU-R (2015) 530–12.

## Appendix

## A. Channel Modelling

We assume that the network operator disposes of two orthogonal frequency bands. One band is assigned to *gBS*s to provide access service to ground users as well as aerial backhaul service to *aBS*s. The other band is assigned to *aBS*s for aerial user access. Hence, we model three different channel types: (i) air-to-ground and (ii) ground-to-ground channels in the access network, and (iii) ground-to-air channels in the backhaul network.

Indeed, the access network communication channels between BSs and UEs differ much depending on whether users connect to a *gBS* or to an *aBS*. While the ground-to-ground channel attenuation for *gBS*–UE links follows conventional path-loss modeling based on slow and fast fading, air-to-ground channels (*aBS*–UE links) suffer additional attenuation depending on the LoS—or NLoS—state of the channel. Such additional attenuation is referred to in the literature as an *excess attenuation* [44]. Moreover, antennas used for the access network differ from backhaul network antennas performing 3D-beamforming, which directly affects the interference suffered in each case. In the following sections, we detail these features for each type of modelled channel.

### *A.1. Air-to-Ground Channels*

Depending on whether links between *aBS*s and UEs are free of obstacles (e.g., buildings, traffic, etc.), the attenuation differs notably [44]. The LoS-likelihood is a complex function of the elevation angle between UE $u \in \mathcal{U}$ and *aBS* $a \in \mathcal{A}$:

$$P_{LoS}(a,u) = \frac{1}{1+\beta_1 \cdot \exp\left(-\beta_2\left(\frac{180}{\pi}\arctan\left(\frac{h_a}{r_{a,u}}\right)-\beta_1\right)\right)}, \tag{2}$$

where the elevation of $a$ is $h_a$, while $\beta_1$ and $\beta_2$ are parameters depending on the number of large signal obstructions per unit area, building's height distribution, ratio of built-up area and clean surfaces, etc., as derived in [45], based on ITU recommendations [69]. In Eq. (2), $\theta_{a,u}$=arctan$(h_a/r_{a,u})$ is the elevation angle. $\theta_{a,u}$ approaches $\frac{\pi}{2}$ when the *aBS* $a$ hovers just above the user $u$, i.e., when the LoS likelihood reaches its maximum. The elevation angle $\theta_{a,u}$ is characterized by the *aBS* height and the ground distance between the user and the *aBS*, that is $r_{a,u} = |(X_a, Y_a) - (x_u, y_u)|$. Since safety, legislation and technology constraints allow drones to fly only at low altitudes—a few hundreds of meters at most—the ground distance can be of the same order of the drone's elevation, so that the argument of the arctan function in Eq. (2) can vary sensibly with user and drone positions, and so can LoS likelihood. This means that drone positions, including their elevation, play an important role on air-to-ground channel conditions.

In particular, the average attenuation (in dB units) of an air-to-ground channel between drone $a$ and user $u$ depends on the LoS likelihood, with the following expression [45]:

$$L_{\mathcal{A}}(a,u) \quad = \quad 20\log_{10}\left(\frac{4\pi f_{\mathcal{A}}}{c}\cdot\sqrt{h_a^2+r_{a,u}^2}\right) + P_{LoS}(a,u)\cdot(\xi_{LoS}-\xi_{NLoS}) + \xi_{NLoS}, \tag{3}$$

where $\xi_{LoS}, \xi_{NLoS}$ are the *excess attenuation* components in LoS/NLoS conditions; $f_{\mathcal{A}}$ is the carrier frequency in Hz; and $c$ is the speed of light in m/s.

Since *gBS*s and *aBS*s operate onto orthogonal bands, there is no interference between drone-served users and cellular users, which is commonly the main limiting factor in aided cellular networks, as, e.g., *inband* D2D networks [15]. With the above, the experienced SINR for air-to-ground access links $(a,u)$ is:

$$\gamma_{a,u}^{\mathcal{A}} = \frac{P_{Tx}^{a}\cdot 10^{-L_{\mathcal{A}}(a,u)/10}}{N_{a,u}+I_{a,u}^{\mathcal{A}}}, \tag{4}$$

where $P_{Tx}^{a}$ is the transmission power of an omnidirectional antenna in the *aBS*s $a \in \mathcal{A}$; $N_{a,u}$ is thermal noise according to the allocated bandwidth; and $I_{a,u}^{\mathcal{A}}$ is the interference level that user $u$ suffers from other *aBS*s. However, note that the 3D position of an *aBS* is a decision parameter that directly affects interfering signals received by user $u$, i.e.:

$$I_{a,u}^{\mathcal{A}} = \sum_{a' \in \mathcal{A} \setminus \{a\}} P_{Tx}^{a} \cdot 10^{-L_{\mathcal{A}}(a',u)/10}, \quad \forall a \in \mathcal{A}, \tag{5}$$

where $L_{\mathcal{A}}(a', u)$ depends on the 3D position of *aBS*s $a' \in \mathcal{A}$, as shown in Eq. (3).

*A.2. Ground-to-Ground Channels.*

Connections in the access network between *gBS*s and users experience an attenuation based on a well-known path-loss model with slow fading (in dB units):

$$L_{\mathcal{G}}(g,u) = 10\eta_{\mathcal{G}} \log_{10}\left(\frac{4\pi f_{\mathcal{G}}}{c_l} \cdot |\Pi^g - \pi_u|\right) + \mathcal{N}(0, \sigma_{\mathcal{G}}^2), \tag{6}$$

where $\eta_{\mathcal{G}} > 2$ is the path-loss exponent in ground communications; $f_{\mathcal{G}}$ is the operating carrier frequency of the *gBS*s; and $\sigma_{\mathcal{G}}$ is the standard deviation of the Gaussian random variable $\mathcal{N}(0, \sigma_{\mathcal{G}}^2)$, modelling the effects of shadowing.

As mentioned above, since there is no interference between cellular users and drone-served users, the SINR for access links $(g, u)$ is:

$$\gamma_{g,u}^{\mathcal{G}} = \frac{P_{Tx}^{g} \cdot 10^{-L_{\mathcal{G}}(g,u)/10}}{N_{g,u} + I_{g,u}^{\mathcal{G}}}, \tag{7}$$

where $P_{Tx}^{g}$ is the transmission power of an omnidirectional antenna integrated in the *gBS*s $g \in \mathcal{G}$; $N_{g,u}$ represents thermal noise according to the allocated bandwidth; and most importantly, $I_{g,u}^{\mathcal{G}}$ is the interference level that user $u$ suffers from other *gBS*s.

*A.3. Ground-to-Air Channels*

The aerial network relays traffic from the *gBS*s by means of LoS backhaul wireless links. Hence, the attenuation of a *gBS*–*aBS* link $(g, a)$ is the following:

$$L_{\mathcal{B}}(g,a) = 10\eta_{\mathcal{B}} \log_{10}\left(\frac{4\pi f_{\mathcal{B}}}{c} \cdot |\Pi^g - \Pi_a|\right) + \mathcal{N}\left(0, \sigma_{\mathcal{B}}^2\right), \tag{8}$$

where $\eta_{\mathcal{B}} \approx 2$ is the path-loss exponent in LoS; $f_{\mathcal{B}}$ is the operating carrier frequency of the backhaul wireless links; and $\sigma_{\mathcal{B}}^2$ is the standard deviation of the Gaussian random variable $\mathcal{N}\left(0, \sigma_{\mathcal{B}}^2\right)$, modeling the effects of shadowing.

Backhaul links operate on the bandwidth shared with user access to *gBS*s. However, as backhaul links perform 3D-beamforming pointing to the air (where *aBS*s hover), the interference between *gBS*-served users and backhaul-served *aBS*s is very limited. Although the majority of the *gBS* radiating power is focused in one direction towards the air thanks to the adoption of 3D-beamforming, non-ideal beam-patterns also radiate energy in other directions. Therefore, the SINR experienced by an *aBS* $a \in \mathcal{A}$ depends also on the direction in which other *gBS*s transmit to other *aBS*s. The SINR experienced by a *gBS*–*aBS* link $(g, a)$ is:

$$\gamma_{g,a}^{\mathcal{B}} = \frac{P_{Tx}^{g} \cdot G_g \cdot 10^{-L_{\mathcal{B}}(g,a)/10}}{N^{g,a} + I_{g,a}^{\mathcal{B}}}, \tag{9}$$

where $P_{Tx}^{g}$ is the transmission power of the *gBS* $g$; $G_g$ is the antenna gain over the main lobe of the beam-pattern of *gBS* $g$; $N^{g,a}$ is the thermal noise; and $I_{g,a}^{\mathcal{B}}$ is the interference coming from the remaining backhaul links of the network.

Backhaul links reuse the spectrum used for ground cellular connections, although using beam-patterns pointing to the air, while antennas that provide service to ground users are pointing mainly to the ground. Hence, we assume that the interference suffered by a backhaul link $(g, a)$ is dominated by the interference from other backhaul links. Hence, the interference suffered by a backhaul link $(g, a)$ is:

$$I_{g,a}^{\mathcal{B}} = \sum_{g' \in \mathcal{G} \setminus \{g\}} P_{Tx}^{g'} \cdot G_{g'}(\phi_{g',a}) \cdot 10^{-L_{\mathcal{B}}(g',a)/10}, \tag{10}$$

where $\phi_{g',a}$ is the angle between the main lobe direction of the antenna of $g'$ and the position of *aBS* $a$. In case a *gBS* $g'$ does no set any backhaul wireless link, this *gBS* will not affect interference, and $P_{Tx}^{g'}$ will be considered as zero.

## B. Robustness of PADD

Figure 18 depicts the CDF of the relative loss due to erroneous user position estimation, i.e., the relative loss of utility due to optimizing drone positions according to erroneous user positions. The figure also shows the error in terms of throughput and fairness separately. The loss is below 10% in all cases, and below 3% for utility and throughput in more than half of the cases, while the average loss is below 5%.

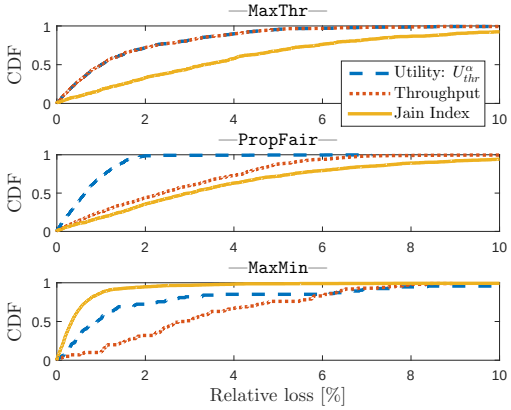


Figure 18: Robustness validation for $\alpha \in \{0, 1, \infty\}$. CDF of the relative loss. $G = 10$, $A = 5$, $U = 1000$. Scenario: *PPP*.